ARMY RESEARCH LABORATORY

ARL

Analytical Simulation and Verification of Air Gun Impact Testing

by Adam Bouland and Mostafiz R. Chowdhury

ARL-TR-3559   **August 2005**

NOTICES

Disclaimers

The findings in this report are not to be construed as an official Department of the Army position unless so designated by other authorized documents.

Citation of manufacturer's or trade names does not constitute an official endorsement or approval of the use thereof.

DESTRUCTION NOTICE—Destroy this report when it is no longer needed. Do not return it to the originator.

Army Research Laboratory

Adelphi, MD 20783-1145

ARL-TR-3559   **August 2005**

Analytical Simulation and Verification of Air Gun Impact Testing

Adam Bouland and Mostafiz R. Chowdhury
Weapons and Materials Research Directorate, ARL

REPORT DOCUMENTATION PAGE

Form Approved
OMB No. 0704-0188

1. REPORT DATE *(DD-MM-YYYY)*	2. REPORT TYPE	3. DATES COVERED *(From - To)*
August 2005	Final	May to December 2004

4. TITLE AND SUBTITLE	5a. CONTRACT NUMBER
Analytical Simulation and Verification of Air Gun Impact Testing	5b. GRANT NUMBER
	5c. PROGRAM ELEMENT NUMBER

6. AUTHOR(S)	5d. PROJECT NUMBER
Adam Bouland and Mostafiz R. Chowdhury (ARL)	622618H80
	5e. TASK NUMBER
	5f. WORK UNIT NUMBER

7. PERFORMING ORGANIZATION NAME(S) AND ADDRESS(ES)	8. PERFORMING ORGANIZATION REPORT NUMBER
U.S. Army Research Laboratory Weapons & Materials Research Directorate Adelphi, MD 20783-1197	ARL-TR-3559

9. SPONSORING/MONITORING AGENCY NAME(S) AND ADDRESS(ES)	10. SPONSOR/MONITOR'S ACRONYM(S)
	11. SPONSOR/MONITOR'S REPORT NUMBER(S)

12. DISTRIBUTION/AVAILABILITY STATEMENT

Approved for public release; distribution is unlimited.

13. SUPPLEMENTARY NOTES

14. ABSTRACT

This report presents an analytical method to simulate the acceleration pulses and forces experienced by test objects during air gun impact testing. The purpose of an air gun impact test is to determine the survivability of sensitive artillery components during launch. It does so by simulating the acceleration pulse and shock waves experienced by such objects during firing. In an air gun impact test, these forces are generated by the impact of a "bird"/test object with an energy-absorbing mitigator complex, which consists of an aluminum honeycomb mitigator and a large momentum exchange mass (MEM). The front of this mitigator is shaped as a wedge or cone, which plastically deforms to provide for a gradual deceleration. Customers often request the peak acceleration they wish to achieve in a given test; therefore, a simulation is necessary to design a test around a client's needs. This report develops a discrete element simulation to predict the acceleration pulse experienced by an object during an air gun test.

The model accounts for the frequency contents of different regions of the test object, which had been simplified to a single frequency or omitted altogether from previous models (*1*). The model also accounts for the elastic and plastic deformation of the aluminum honeycomb mitigator. The strain rate dependency of the plastic crush force is derived with experimental data, confirmed with reference materials, and integrated into the model. A plastic wave front is tracked through the geometry of the mitigator, and the inertial mass transfer of the crushed portion of the mitigator from the MEM complex to the "bird" is accounted for as well. After the crush phase is complete, the mitigator is allowed to elastically unload. This model is governed by a damped spring mass system in which the mitigator is represented as a dynamic force. The stiffness of the components is derived geometrically. The simulation is programmed into Visual Basic[1] via a finite difference time-stepping scheme. Results of the model are verified by comparison with actual test results as well as previous simulations. The new model accurately predicts the peak acceleration pulse, the duration of the acceleration pulse, and the frequency content of the test and shows significant improvement over previous models. [1]Visual Basic is a registered trademark of Microsoft.

15. SUBJECT TERMS

air gun test; finite difference method; honeycomb mitigator; spring mass system

16. SECURITY CLASSIFICATION OF:			17. LIMITATION OF ABSTRACT	18. NUMBER OF PAGES	19a. NAME OF RESPONSIBLE PERSON Adam Bouland
a. REPORT	b. ABSTRACT	c. THIS PAGE	SAR	55	19b. TELEPHONE NUMBER *(Include area code)*
Unclassified	Unclassified	Unclassified			301-394-6308

Standard Form 298 (Rev. 8/98)
Prescribed by ANSI Std. Z39.18

Contents

List of Figures

Acknowledgments

INTENTIONALLY LEFT BLANK

1. Introduction

The U.S. Army Research Laboratory (ARL) has long used air gun testing to assist in the development of weapons systems and technologies. The purpose of the test is to simulate the acceleration pulse and shock waves experienced by artillery components during launch. This allows the defense industry to test the survivability of individual artillery components for less than the cost of an actual field test. Such tests allow defense contractors to identify the weak components of their weapons design and to better understand the behavior of their components during launch.

Department of Defense (DoD) clients often specify the acceleration/shock conditions they wish to achieve in a given test. For instance, they may request the peak acceleration or the duration of the acceleration pulse. Researchers at ARL have no direct control over the acceleration pulse; it is therefore necessary to mathematically model the air gun test to predict the acceleration pulse delivered by a specific test. ARL can then modify the initial parameters of the air gun tests in order to shape the acceleration pulse to match the conditions requested by the client.

The current simulation used by ARL in conducting its tests treats all components in the test as rigid bodies (*2*). Such a simplified model fails to capture the high-frequency oscillations experienced by the test objects and the true peak acceleration of the test. This report develops an extension of work done by Tabei and Chowdhury (*1*) by adding two degrees of freedom to the system, thus allowing ARL to account for the varying properties of the test objects in its test design. The resulting simulation uses the initial parameters and material properties of a test to predict the acceleration pulse and displacements experienced by a given component, allowing ARL to better satisfy the demands of DoD clients and extending the development capability of the defense community.

2. Air Gun Testing/Simulation Setup

2.1 Air Gun Test Setup

A diagram of the test setup is presented in figure 1. The air gun test achieves its desired acceleration pulse through the impact of a "bird" with an energy-absorbing mitigator. The bird consists of a test object mounted on an on-board recorder (OBR) which measures the acceleration pulse produced by the test. This bird is fired by compressed gas (usually helium or air) down an evacuated firing tube and into a "catch" tube. There, the bird impacts an aluminum honeycomb mitigator which crushes to absorb the energy of the impact. The remaining energy is then transferred to a large momentum exchange mass (MEM) which is displaced by the inertial force of the system.
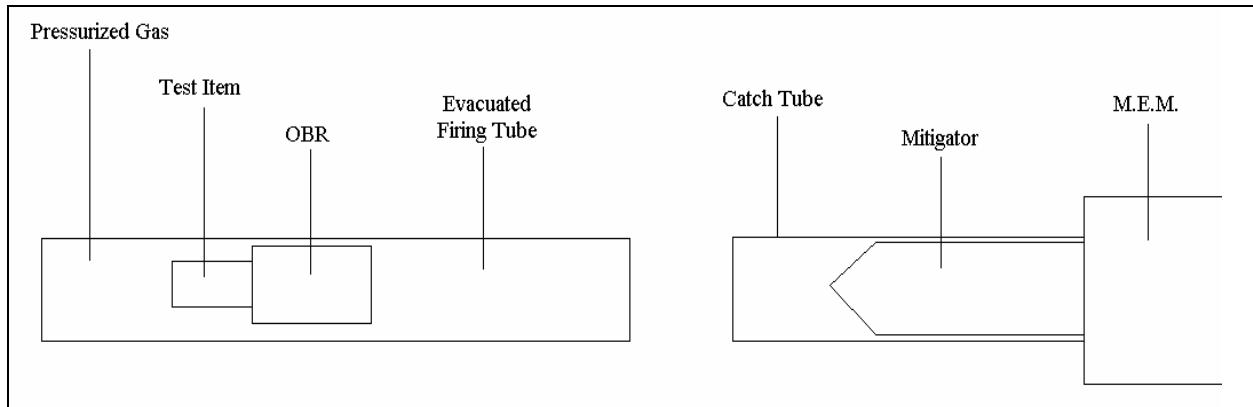
Figure 1. Air gun test setup.

The OBR used in these tests consists of two steel plates connected by a hollow aluminum cylinder. The area inside the OBR is filled with glass beads that surround an accelerometer, damping the high-frequency oscillations of the OBR. The test object is mounted on the back plate of this OBR. The mitigator used in this test is shaped with a double-wedged front, but other mitigator geometries are also used. These tests are conducted in a variety of air guns, ranging from 2 to 7 inches in diameter.

2.2   Firing Procedure

After the OBR and test object are assembled and secured together, the bird is loaded into the breech of the air gun. The bird is held in place by two identical firing pins which are specially machined to yield at a certain force. The air gun is then sealed, and a large gas tank is brought into position behind the bird. Once the firing tube has been evacuated, compressed gas is gradually loaded into the tank behind the bird. Pressure measurements are taken periodically. As the pressure in the tank increases, the force exerted on the bird eventually reaches the yield stress of the firing pins. The pins break, releasing the bird and allowing the pressurized gas to propel it down the firing tube. The bird's velocity is measured at the end of the firing tube, and its acceleration is measured by the OBR during impact.

2.3   Simulation Setup

In order to model the air gun impact analytically, it is necessary to divide the air gun apparatus into discrete elements. The elements selected in figure 2 are designed to increase the accuracy of the model without overly complicating the model or drastically increasing computer run time. The OBR consists of three discrete elements in order to model its physical construction. The front plate, back plate, and test object are designated as point masses while the hollow cylinder and test object connection are modeled as damped springs with their own stiffness. A process for deriving the stiffness of these objects through geometric means is detailed in section 4 of this report, while frequency extraction and finite element (FE) simulation methodologies are detailed in section 5.

2
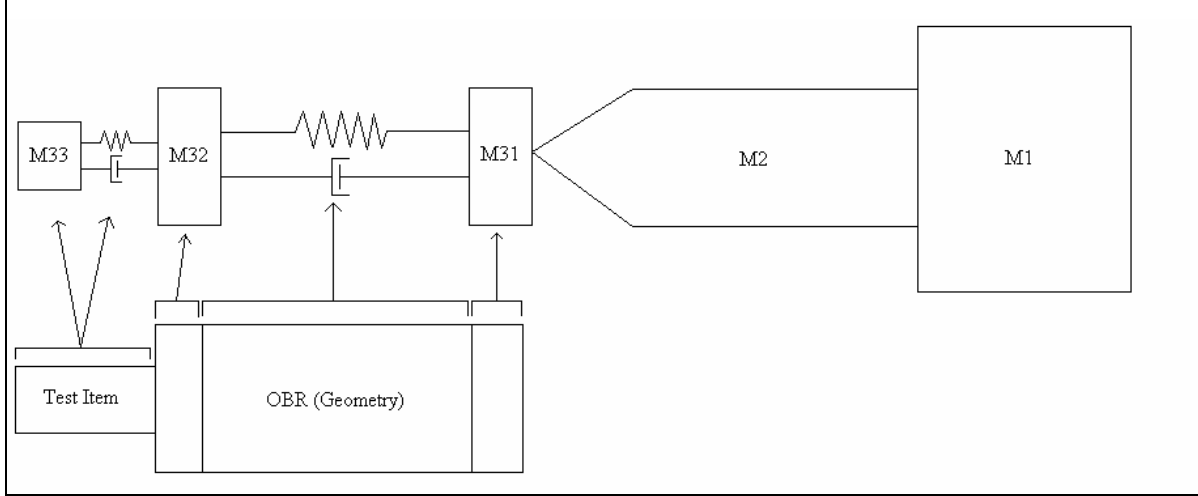
Figure 2. Simulation setup. (Note: Although conical mitigators are represented in the diagrams, double-wedged mitigators were used in the actual tests.)

3. Mathematical Construction of the Model

3.1 Basic System of Equations

A system of equations can be easily formulated to govern the behavior of the discrete model. To generate these equations, the model is divided into four sections, each of which governs the motion of one mass. Figure 3 presents the discretization of the model. At any given time, the net forces on these masses must equal 0, since every force must have an equal and opposite counter-force. The inertial forces of the masses are given by F = ma; damping forces are given by F = cv, in which c is the damping coefficient and v is the relative velocity of the masses; and spring forces are given by F = ku, in which k is the stiffness of the spring and u is its displacement. The force exerted by the mitigator is detailed in the next section.
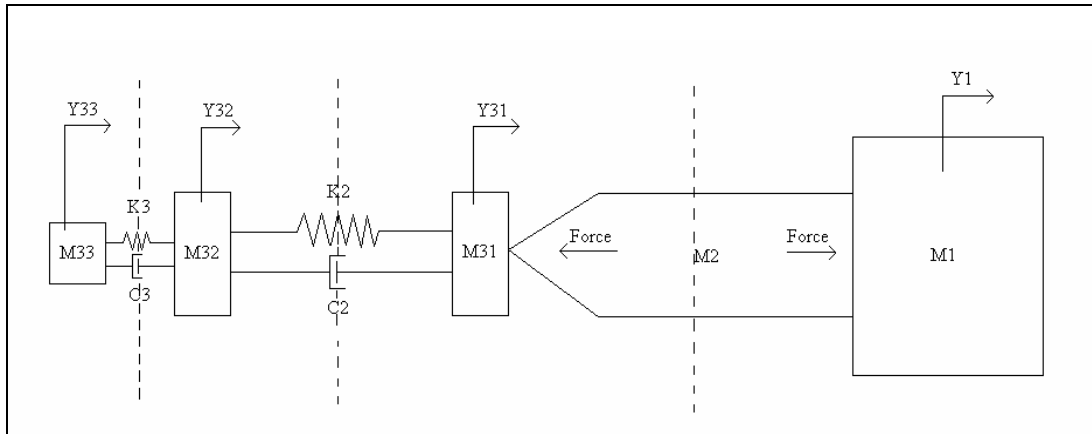
Figure 3. Mathematical diagram of the model.

Let $Y_1 - Y_{33}$ be the displacements of m_1 - m_{33}, respectively, let $\dot{Y}_1 - \dot{Y}_{33}$ be the velocities of $m_1 -$ m_{33}, respectively, and let $\ddot{Y}_1 - \ddot{Y}_{33}$ be the accelerations of $m_1 - m_{33}$, respectively. It therefore follows that

$$F_{mitigator} - (m_1 + m_2)\ddot{Y}_1 = 0$$
$$(m_{31}\ddot{Y}_{31}) - F_{mitigator} + k_2(Y_{31} - Y_{32}) + c_2(\dot{Y}_{31} - \dot{Y}_{32}) = 0$$
$$(m_{32}\ddot{Y}_{32}) - k_2(Y_{31} - Y_{32}) + k_3(Y_{32} - Y_{33}) - c_2(\dot{Y}_{31} - \dot{Y}_{32}) + c_3(\dot{Y}_{33} - \dot{Y}_{32}) = 0$$
$$(m_{33}\ddot{Y}_{33}) - k_3(Y_2 - Y_{33}) - c_3(\dot{Y}_{32} - \dot{Y}_{33}) = 0$$

$$(1)$$

This system of equations is more easily represented by the matrices

$$
\begin{bmatrix} m_1+m_2 & 0 & 0 & 0 \\ 0 & m_{31} & 0 & 0 \\ 0 & 0 & m_{32} & 0 \\ 0 & 0 & 0 & m_{33} \end{bmatrix}
\begin{Bmatrix} \ddot{Y}_1 \\ \ddot{Y}_{31} \\ \ddot{Y}_{32} \\ \ddot{Y}_{33} \end{Bmatrix} +
\begin{bmatrix} 0 & 0 & 0 & 0 \\ 0 & c_2 & -c_2 & 0 \\ 0 & -c_2 & c_2+c_3 & -c_3 \\ 0 & 0 & -c_3 & c_3 \end{bmatrix}
\begin{Bmatrix} \dot{Y}_1 \\ \dot{Y}_{31} \\ \dot{Y}_{32} \\ \dot{Y}_{33} \end{Bmatrix} +
\begin{bmatrix} 0 & 0 & 0 & 0 \\ 0 & k_2 & -k_2 & 0 \\ 0 & -k_2 & k_2+k_3 & -k_3 \\ 0 & 0 & -k_3 & k_3 \end{bmatrix}
\begin{Bmatrix} Y_1 \\ Y_{31} \\ Y_{32} \\ Y_{33} \end{Bmatrix} =
$$

$$(2)$$

$$
\begin{Bmatrix} F_{mitigator} \\ -F_{mitigator} \\ 0 \\ 0 \end{Bmatrix}
$$

or

$$[M]\{\ddot{Y}\} + [C]\{\dot{Y}\} + [K]\{Y\} = \{F_{mitigator}\}$$

$$(3)$$

This equation governs the motion of the model during the time step.

3.2 Representation of Mitigator Behavior

The mathematical representation of the mitigator is crucial to the overall accuracy of the model. As illustrated by the honeycomb stress/strain diagram in figure 4, the mitigator offers a short period of elastic resistance followed by a longer period of plastic deformation. This area of plastic deformation does not occur at the front of the OBR but rather at the front of a plastic wave traveling through the mitigator. Figure 5 illustrates the air gun test during this crush phase of the mitigator. The force exerted by the plastic deformation of the mitigator is proportional to the cross-sectional area of the mitigator at the plastic wave; therefore, the position of the plastic wave must be tracked. The speed of the plastic wave is given by (1)

$$C_{plastic} = (V_{OBR/MEM}) / \varepsilon_c$$

$$(4)$$

in which ε_c is the compacting strain of the honeycomb and $V_{OBR/MEM}$ is the relative velocity of the OBR and MEM, given by V_{OBR} - V_{MEM}. The position of the plastic wave front is therefore easily revised each time step through equation 4

$$X_{plastic(n)} = X_{plastic(n-1)} + C_{plastic} * \Delta t$$

$$(5)$$

4
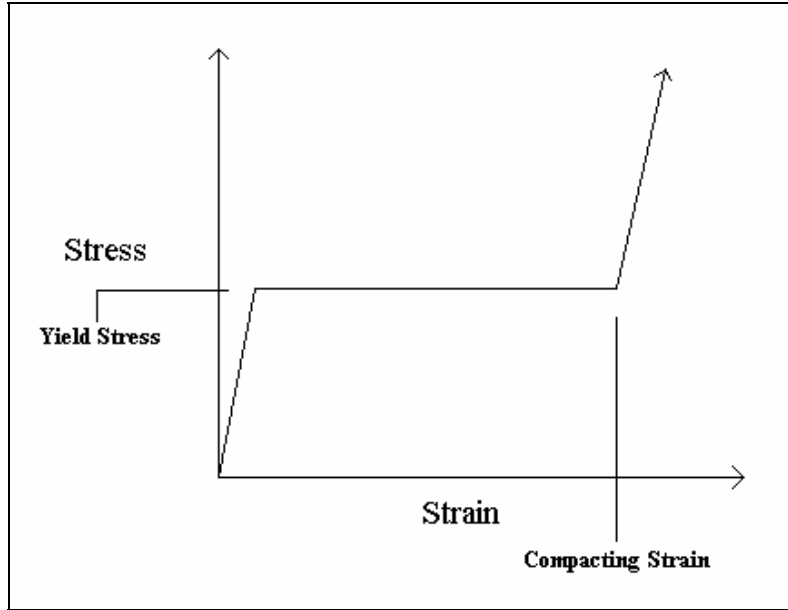
Figure 4. Stress-strain diagram of aluminum honeycomb (*1*).
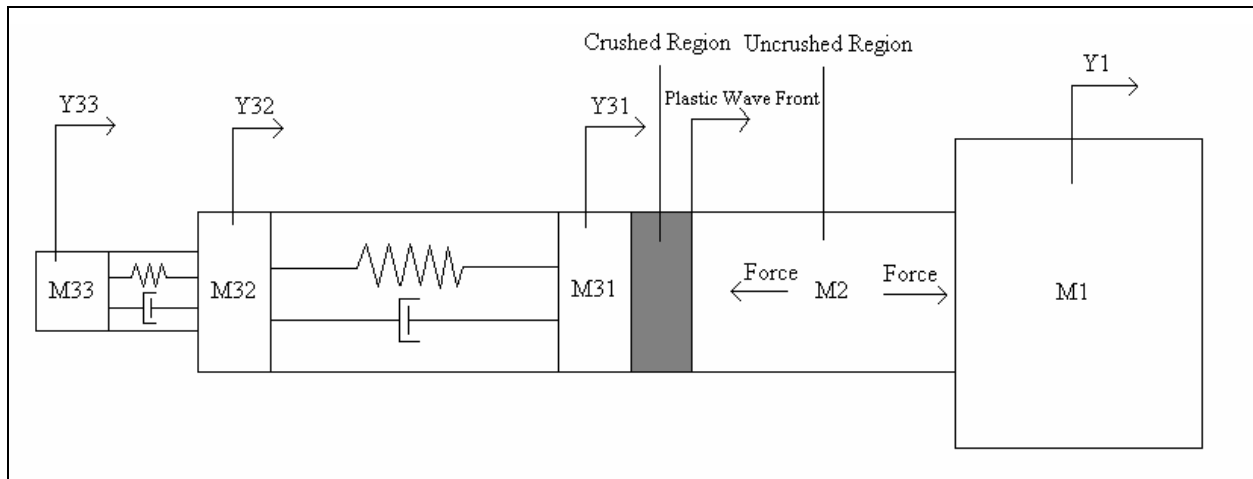
Figure 5. Mid-shot view of the model.

During the initial crush phase of the mitigator, the elastic resistance offered by the honeycomb is negligible because the energy absorbed by elastic deformation is extremely low. While the mitigator is crushing, the strain on the honeycomb far exceeds its yield strain, thus absorbing much more energy (given by the area under the stress-strain curve) through plastic rather than elastic deformation. The elastic resistance of the mitigator is therefore ignored during the crushing phase of mitigator deformation.

During this period of plastic deformation, the inertial masses of the OBR and MEM are constantly changing (*2*). As the plastic wave front advances, the crushed portion of the mitigator acquires the velocity of the OBR and therefore behaves as part of the inertial mass of the front plate of the OBR. Likewise, the MEM complex loses inertial mass to the crush front as the

plastic wave progresses. We account for this inertial mass transfer by calculating the volume of mitigator transferred from the MEM/mitigator to the OBR front plate and multiplying by the density of the mitigator ($\rho_{mitigator}$).

The calculation of the force associated with the plastic deformation of the mitigator must take into account the dynamic crush force of the mitigator. In a static model, the crush force would be given by (*1*)

$$F_{mitigator} = \sigma_y * A \qquad\qquad (6)$$

in which σ_y is the static yield stress of honeycomb and A is the cross-sectional area of the mitigator at the plastic wave front. This area varies with the position of the wave front. However, in a dynamic model, the crush force is related to the strain rate of the honeycomb (which is a function of the relative velocity of the OBR and mitigator) (*3*).

In order to determine the relationship between the percent increase in crush force and the velocity, experimental acceleration data from two test shots were multiplied by the mass of the components to receive a time history of the mitigator force. The masses of the components were assumed to be constant, and the resulting increase in crush force was compared with the components' velocities gathered from the simulation. Figure 6 presents the results of this analysis. The results clearly indicate a discrepancy between the percent increase in crush force between the high-velocity and low-velocity test shots at velocities less than 100 m/s. The crush force of the high-velocity shot is actually less than its static crush force at velocities around 30 m/s, when it should have shown an increased crush force. Since the initial velocity and masses of the low-velocity shot are known, its strain rate dependency during the initial stage of impact (velocities around 85 m/s) is accurate. The strain rate dependency of the high-velocity shot at this velocity clearly falls below the known strain rate dependency of the low-velocity test shot. This clearly reveals the need for inertial mass transfer in the model, which would increase the mass of the OBR toward the end (lower velocities) of the high-velocity shot, thus allowing the strain rate dependency curves to converge.

In order to account for the inertial mass transfer between components, the crush force function was passed through the simulation to create a time history of the masses and velocities of the components. These data were used to create a new model of the strain rate dependency of the mitigator, which was passed through the simulation again. This methodology created a limiting process, allowing the strain rate dependency and the mass transfer functions to converge to within a 1% error within four iterations. Figure 7 presents the results of this analysis. The resulting strain rate dependency functions of each of the tests shots were combined to create a new strain rate dependency curve, which was then approximated with the regression curve shown in figure 8. Notice that the two curves converged after the inertial mass transfer of the components was accounted for.
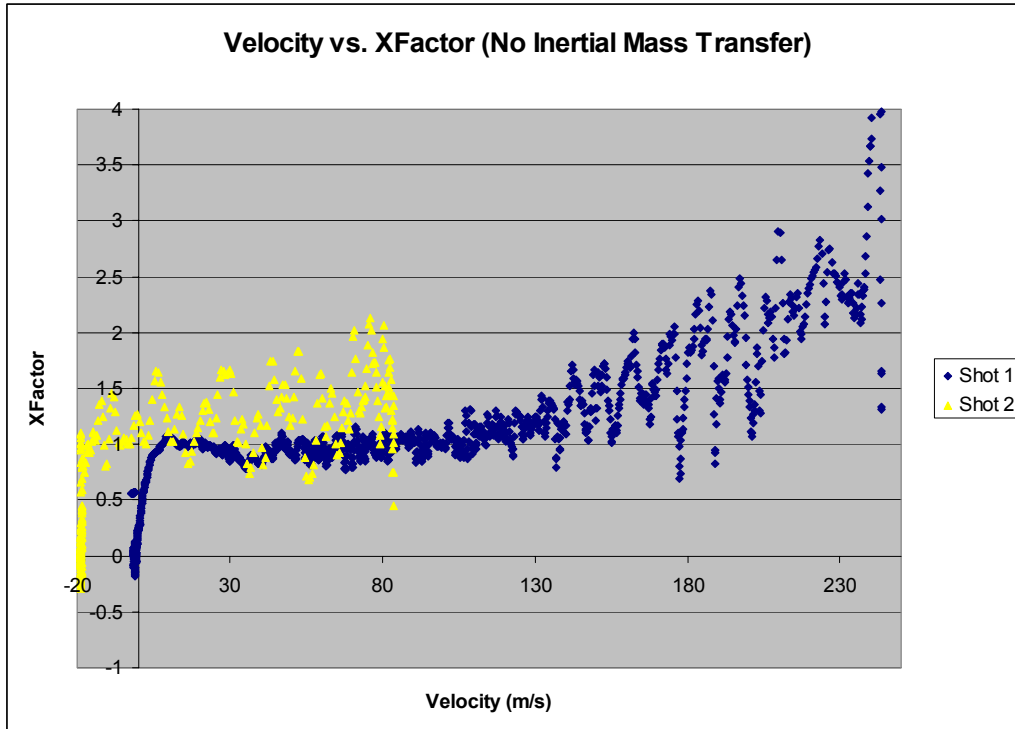
Figure 6. Amplification of crushing force as a function of velocity.
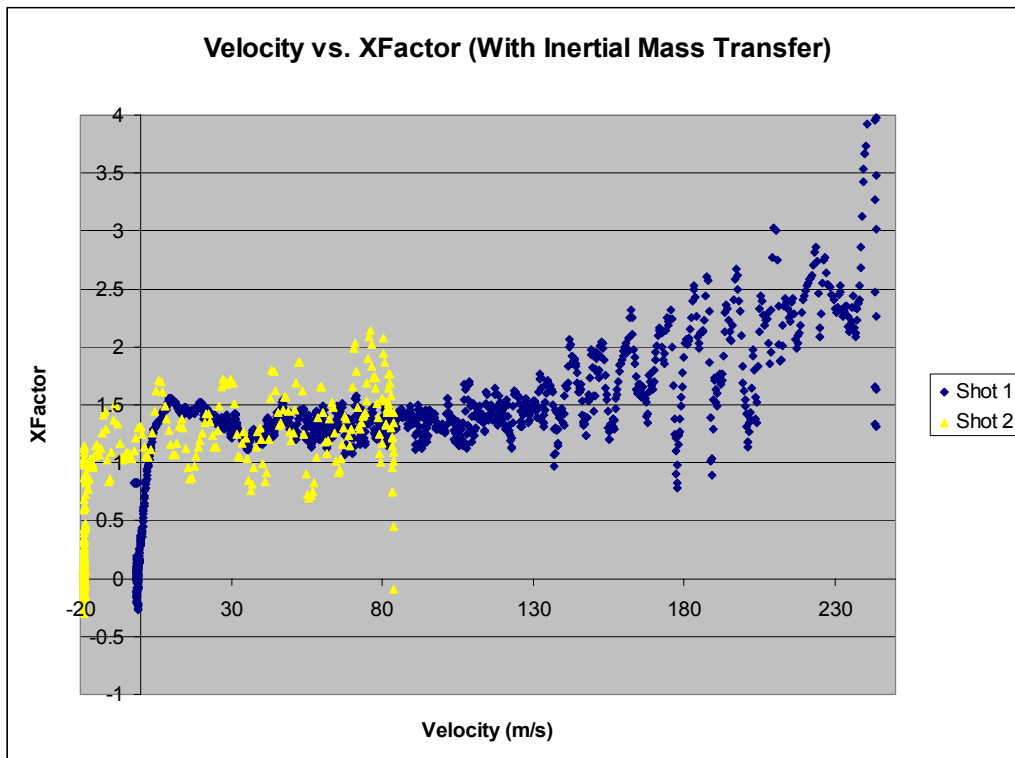
Figure 7. Amplification of crushing force as a function of velocity, with inertial mass transfer.
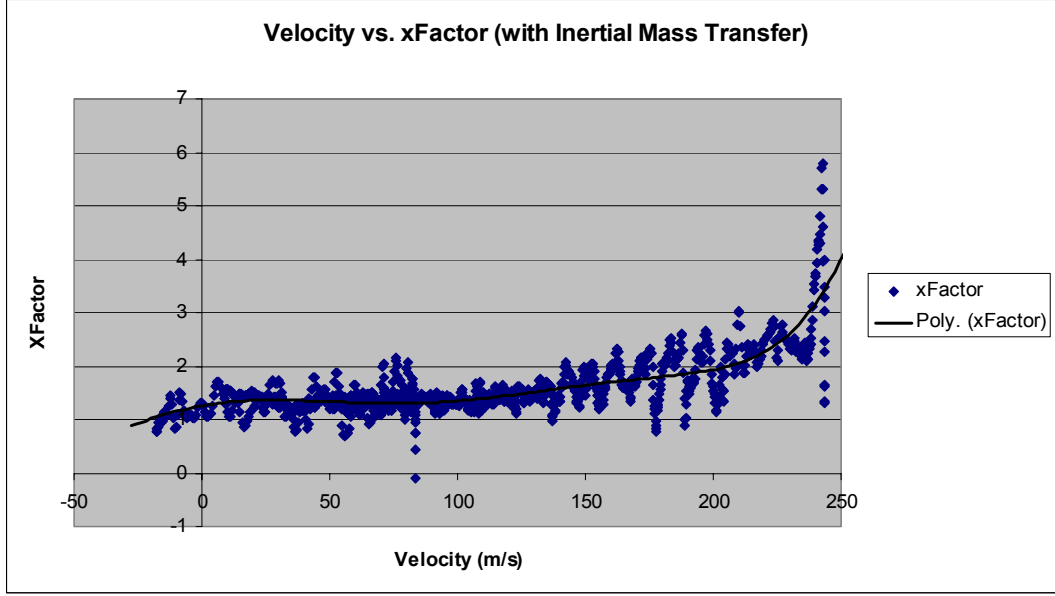
Figure 8. Polynomial approximation of amplification of crushing force.

The strain rate dependent crush force of the mitigator was thus given by

$$F_{mitigator} = X_{factor} * \sigma_y * A \qquad (7)$$

in which X_{factor} was given by a polynomial approximation of the strain rate dependency of the crush force

$$X_{factor} = (2.627E\text{-}13)v^6 - (1.254E\text{-}10)v^5 + (1.592E\text{-}8)v^4 + (5.552E\text{-}7)v^3 - (1.897E\text{-}4)v^2 +$$

$$0.00834v+1.258 \qquad (8)$$

in which v is the instantaneous relative velocity of the OBR and MEM.

Once the mitigator has reached its maximum plastic deformation, it ceases to exert its crush force on the OBR. Therefore, the mitigator force becomes equal to the force of elastic unloading rather than plastic deformation. The stiffness of the remaining mitigator is easily calculated by the formula k = AE/L, and the resulting force is

$$F_{mitigator} = [(A * E) / (L_{mitigator} - X_{plastic})] * (Y_{31} - Y_1) \qquad (9)$$

in which E is the elastic modulus of the mitigator. This force is time stepped to provide a gradual fall from the peak mitigator deformation force.

3.3   Time Stepping the Model

With the physics of the mitigator established, the model is time stepped with a Taylor series to approximate the previous accelerations of the masses. This allows us to develop a central

difference time-stepping method (1). First, a Taylor series is expanded in either direction from a basic position function:

$$\{Y\}_{n+1} = \{Y\}_n + \Delta t \{\dot{Y}\}_n + (\Delta t^2/2)\{\ddot{Y}\}_n \qquad (10)$$

$$\{Y\}_{n-1} = \{Y\}_n - \Delta t \{\dot{Y}\}_n + (\Delta t^2/2)\{\ddot{Y}\}_n \qquad (11)$$

By adding equations 11 and 12, and solving for $\{\ddot{Y}\}_n$, we receive

$$\{Y\}_{n+1} + \{Y\}_{n-1} = 2\{Y\}_n + \Delta t^2 \{\ddot{Y}\}_n \qquad (12)$$

$$\{\ddot{Y}\}_n = (1/\Delta t^2)(\{Y\}_{n+1} - 2\{Y\}_n + \{Y\}_{n-1}) \qquad (13)$$

In order to time step the model, we plug this approximation of $\{\ddot{Y}\}_n$ back into our original formula:

$$[M]\{\ddot{Y}\}_n + [C]\{\dot{Y}\}_n + [K]\{Y\}_n = \{F_{mitigator}\} \qquad (14)$$

$$[M]\{(1/\Delta t^2)(\{Y\}_{n+1} - 2\{Y\}_n + \{Y\}_{n+1})\} = \{F_{mitigator}\} - [K]\{Y\}_n - [C]\{\dot{Y}\}_n \qquad (15)$$

Solving for $\{Y\}_{n+1}$, we receive the equation

$$\{Y\}_{n+1} = 2\{Y\}_n - \{Y\}_{n-1} + \Delta t^2 [M]^{-1}(\{F_{mitigator}\} - [K]\{Y\}_n - [C]\{\dot{Y}\}_n) \qquad (16)$$

in which $\{\dot{Y}\}_n$ is approximated by

$$\{\dot{Y}\}_n = (\{Y\}_n - \{Y\}_{n-1})/\Delta t \qquad (17)$$

This time-stepping equation is implemented in the Visual Basic[1] program in the program section of appendix A. The program tracks the plastic wave propagation and uses these formulas and considerations to time step the positions of the model. Displacement results are recorded directly to an Excel[2] chart. The program then calculates the instantaneous velocities and accelerations of the particles, based on their positions. It also calculates a filtered acceleration curve based on displacement measurements taken at a certain frequency for comparison with rigid body models. The program can be easily modified to track other variables of the simulation, such as the plastic wave front, deformation force of the mitigator, and the inertial masses of the OBR and MEM. This example implements a time step of 0.5 microsecond with a run time of approximately 90 seconds. If computer run time is an issue, the time step and run time can be reduced tenfold from within Excel without sacrificing the simulation's accuracy.

---

[1]Visual Basic is a registered trademark of Microsoft.
[2]Excel is a trademark of Microsoft Corporation.

4. Verification of the Current Model

4.1 Initial Parameters

In order to verify the accuracy of this model, the results of the simulation were compared to those of an actual air gun test (shot A, 7-inch air gun, ARL, Adelphi Laboratory Center). This test was designed to determine the accuracy of a client's OBR, which was relatively geometrically simple. The test therefore easily fit into the framework of the simulation. The initial parameters of the test were provided by ARL staff and converted into kilogram-meter-second units for easy comparison with other research institutions. Other parameters such as the material properties of the honeycomb were extracted from a previous air gun report. The mass distributions within the OBR were obtained through the direct massing of the various bird components. The k-values used in the simulation were calculated on the basis of the OBR's geometry, as depicted in figure 9. The simulation treated the hollow aluminum cylinder as the spring between m_{31} and m_{32} and calculated its stiffness as

$$k_2 = (A * E) / L$$
$$= (17.119 \text{ in}^2)(1.0*10^7 \text{ lb/in}^2) / (5.00 \text{ in}) = 3.42 * 10^7 \text{ lb/in} = 6.08 * 10^9 \text{ N/m}$$

Unfortunately, the geometry of the test item was unavailable. Therefore, the value of k_3 was estimated as roughly twice the value of k_2 because of its unknown steel/aluminum composition. Further methods for discovering k-values are detailed in section 5 of this report.
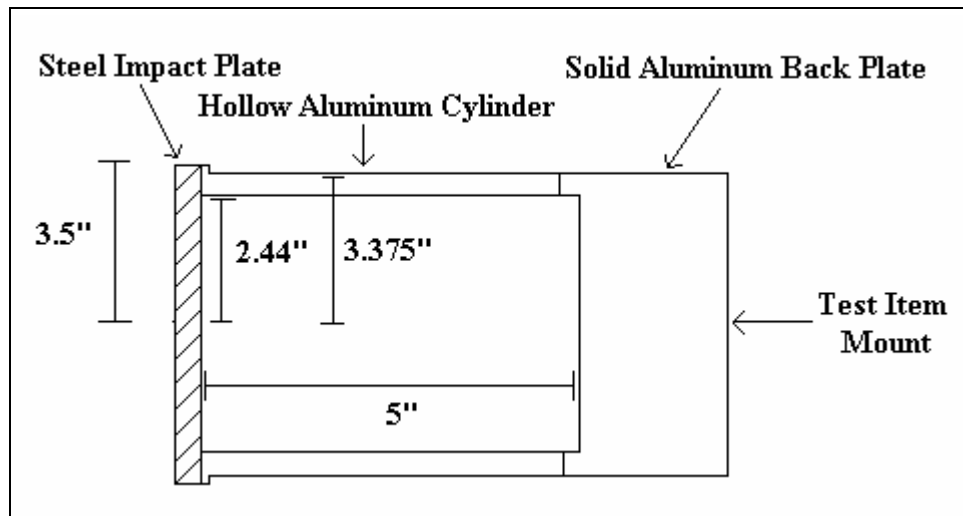

Figure 9. OBR geometry.

We calculated the c-values used in this simulation by modeling the system as an under-damped spring mass system. Therefore, the c-values were given by (*4*)

$$c = 2\sqrt{km}\zeta \qquad (18)$$

In equation 18, m represents the mass assigned to the node assuming a uniform distribution (*4*). Damping was set at 5%, so $\zeta = 0.05$. Following are the initial conditions entered into the analysis:

$m_1 = 559.86$ kg	$E = 4060$ MPa
$m_{31} = 4.01$ kg	$\sigma_y = 27.03$ MPa
$m_{32} = 4.52$ kg	$\varepsilon_c = 0.64$
$m_{33} = 4.53$ kg	$L_{wedge} = 0.098$ m
$k_2 = 6.08 * 10^9$ N/m	$L_{cylinder} = 0.803$ m
$k_3 = 12.16 * 10^9$ N/m	$r_{mitigator} = 0.088$ m
$\rho_{mitigator} = 385$ kg/m^3	$v_0 = 243.5$ m/s

4.2   Results

The actual acceleration of the test object is presented in figure 10. Figure 11 presents the prediction of the previous rigid body model, and figure 12 presents the prediction of the model developed in this report. Figure 13 provides a comparison of the actual and predicted accelerations. Figures 14 and 15 present the fast Fourier transforms of the predicted and test accelerations for frequency content analysis. Figures 16, 17, and 19 present time histories of the mitigator force, mitigator deflection/plastic wave front position, and OBR velocity gathered from the analysis, respectively. Figure 18 presents pictures of the post-shot mitigator.

4.3   Analysis

The results of the simulation reveal that the current model accurately predicts the amplitude and duration of the acceleration pulse of the test. The actual test produced a peak acceleration of 12.27 kG's (1,000 g's) (11.94 kG's filtered), the current model produced a peak acceleration of 11.99 kG's, and the previous model produced a peak acceleration of 10.37 kG's. The current model also accurately predicted the time when this peak pulse occurred; both the current model and the actual test data placed the peak acceleration at around 0.3 ms after impact, while the previous model placed the peak acceleration at 0.4 ms. Both the current and previous models placed the duration of the acceleration pulse at around 5 ms. Most importantly, the current model successfully accounted for the high-frequency oscillations that occur at impact; both the current model and the actual test results showed high-frequency oscillations of approximately the same frequency, while the previous model showed none. This is most clearly demonstrated by the oscillations during the initial increasing acceleration and at the peak of the pulse, which occur at approximately 0.12, 0.3, and 0.42 ms, respectively, in both the current model and test results. The amplitude and frequency of these oscillations were the primary factor responsible for the 13% difference in the peak acceleration of the previous and current models.
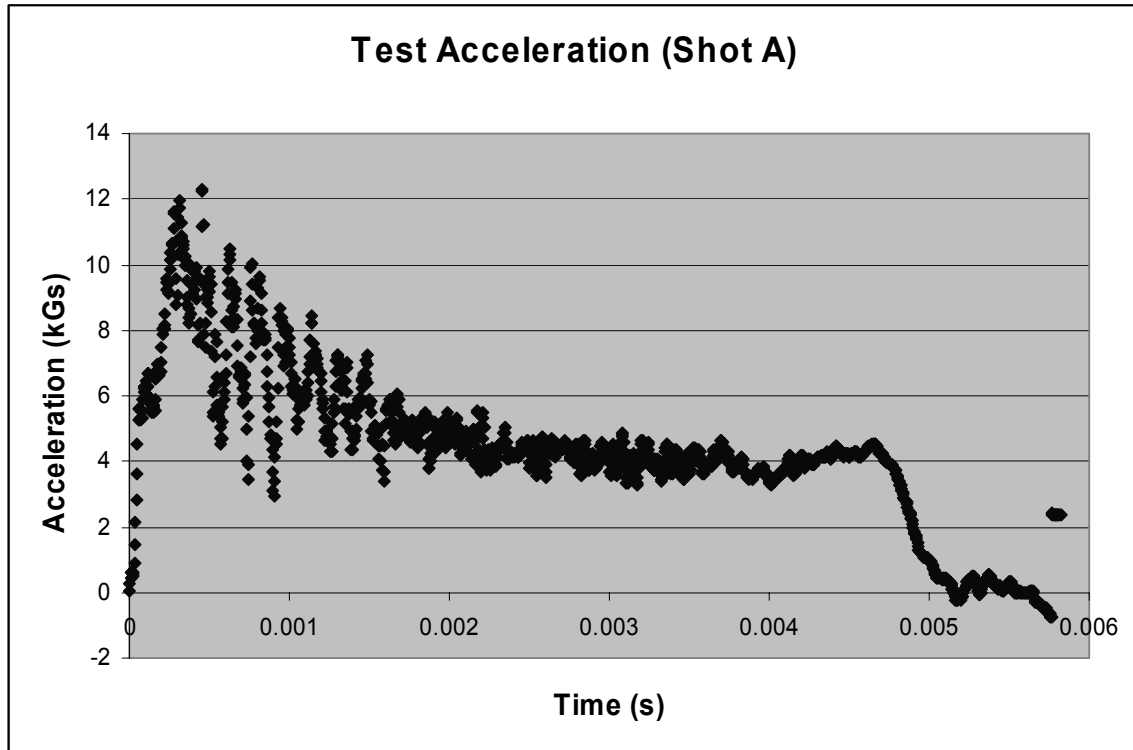
Figure 10. Actual test results.
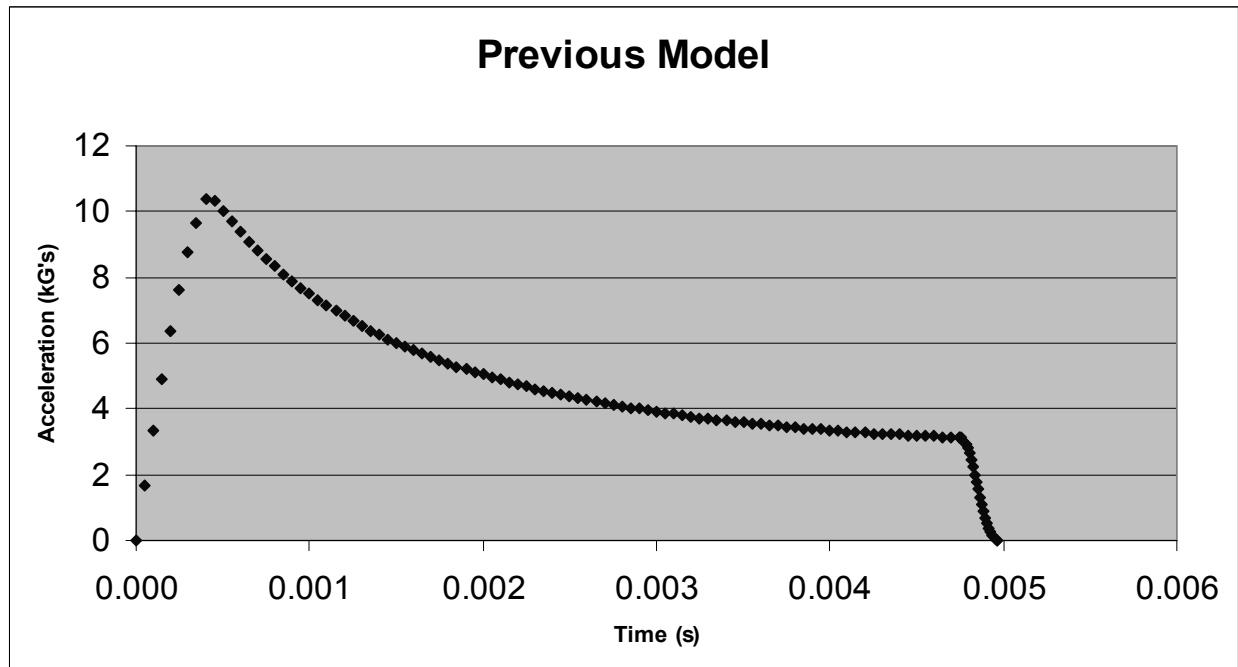
Figure 11. Previous model's prediction.
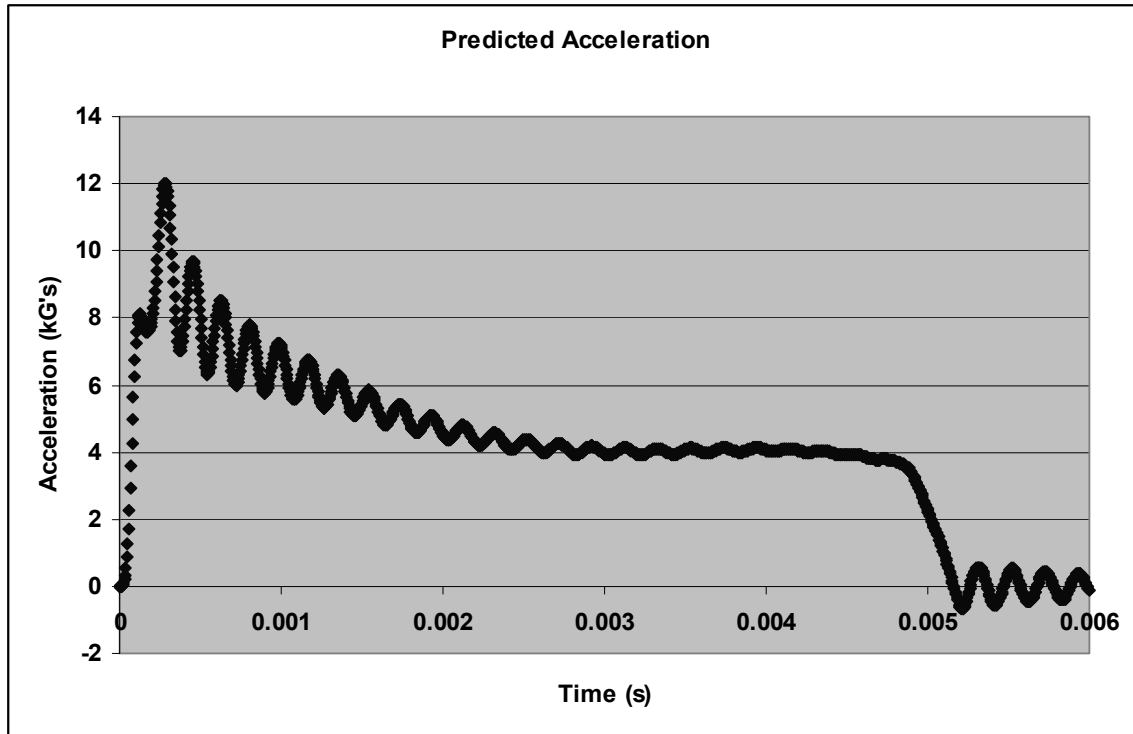
Figure 12. Current model's prediction.
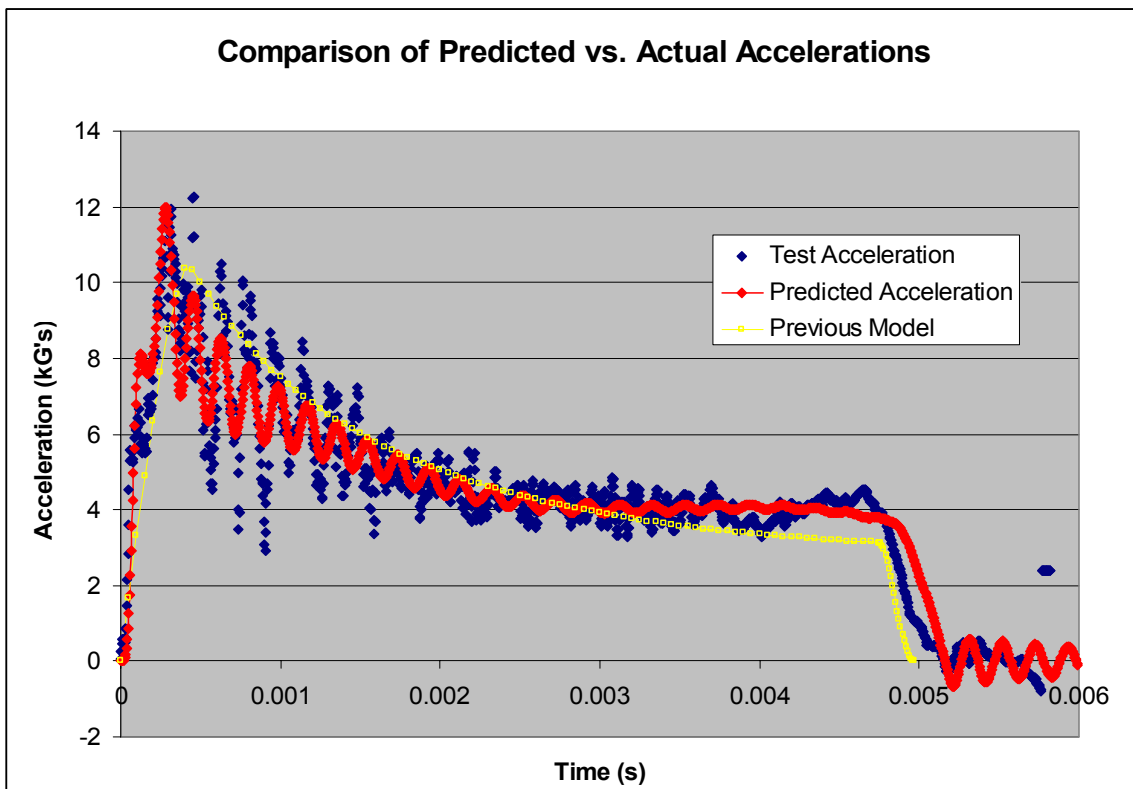
Figure 13. Comparison of test, current model, and previous model acceleration pulses.

13
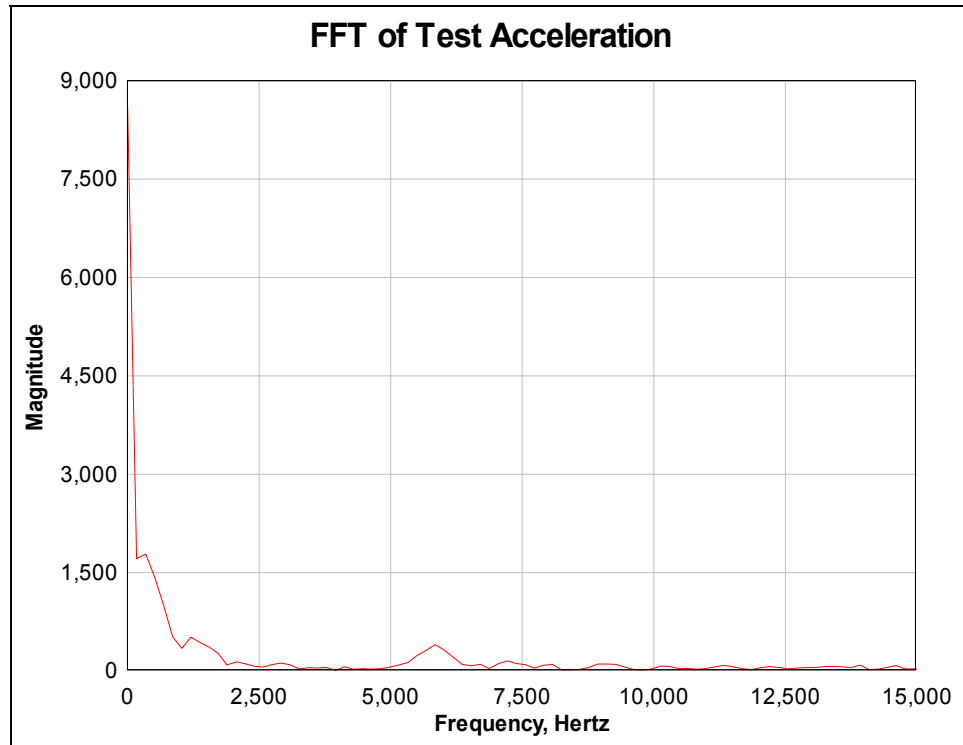
Figure 14. Fast Fourier transform of test acceleration.
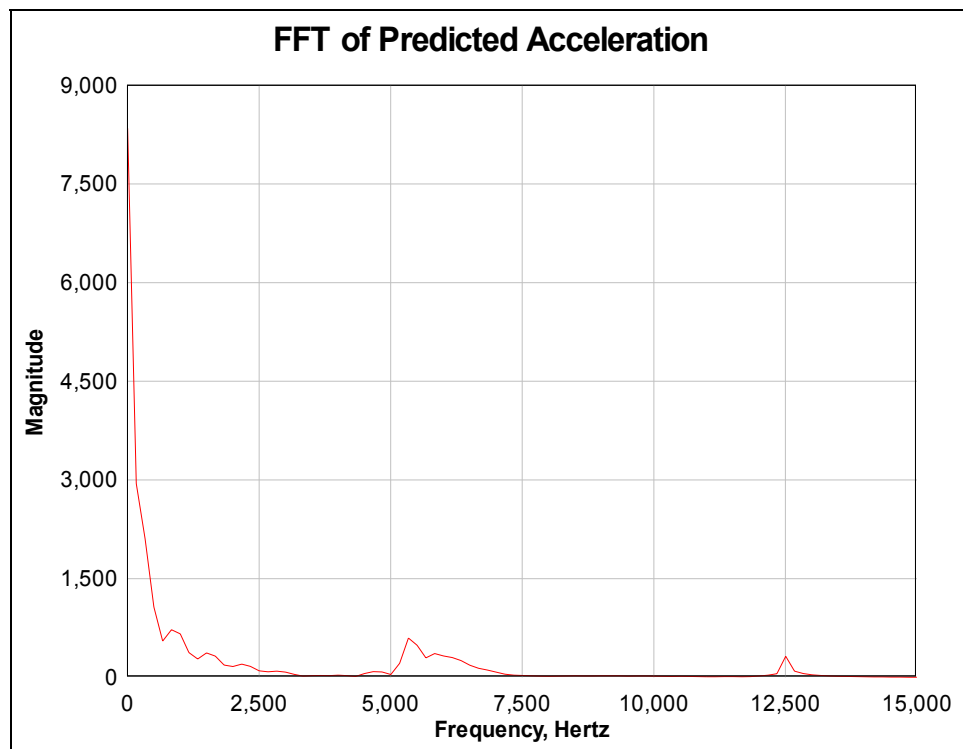
Figure 15. Fast Fourier transform of predicted acceleration.
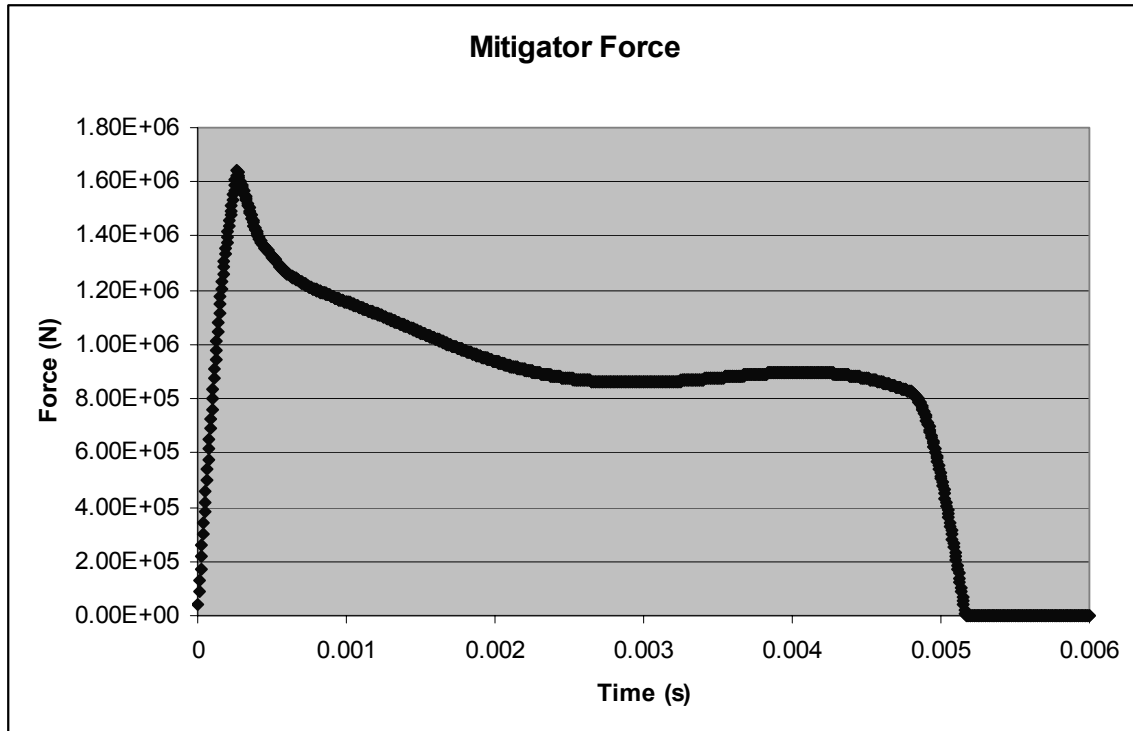
Figure 16. Time history of mitigator force.
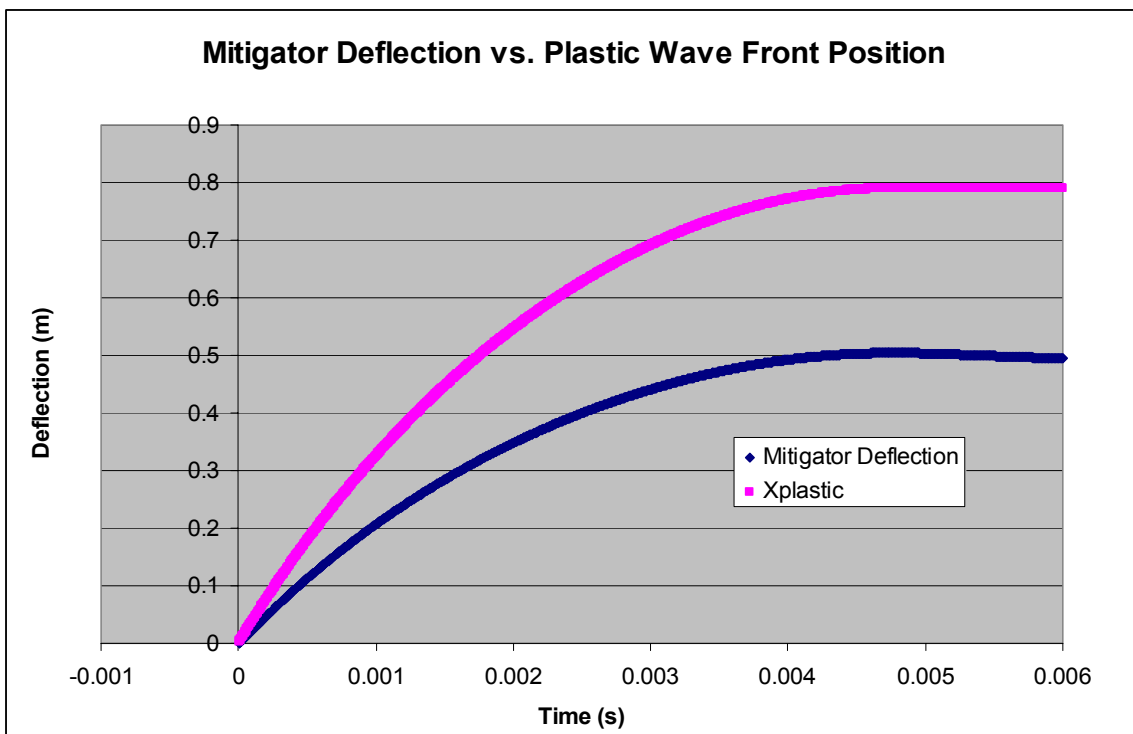
Figure 17. Plastic wave front progression compared to mitigator deflection.
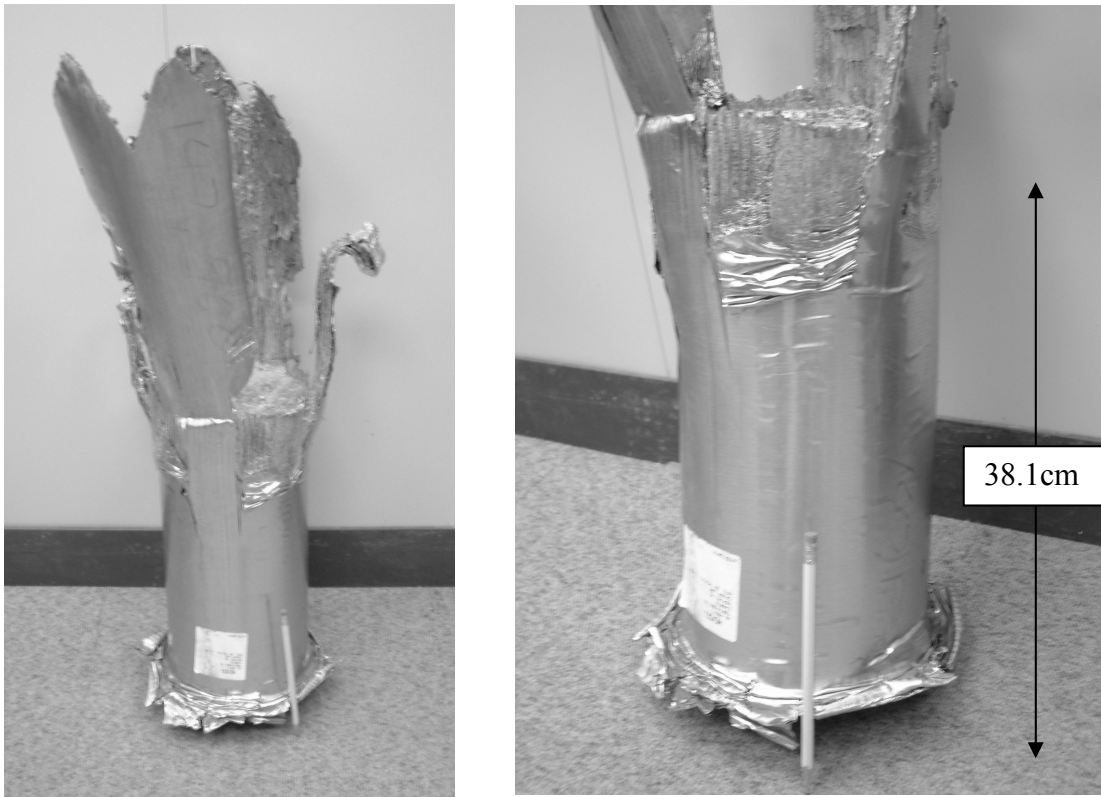
Figure 18. Pictures of post-shot mitigator.
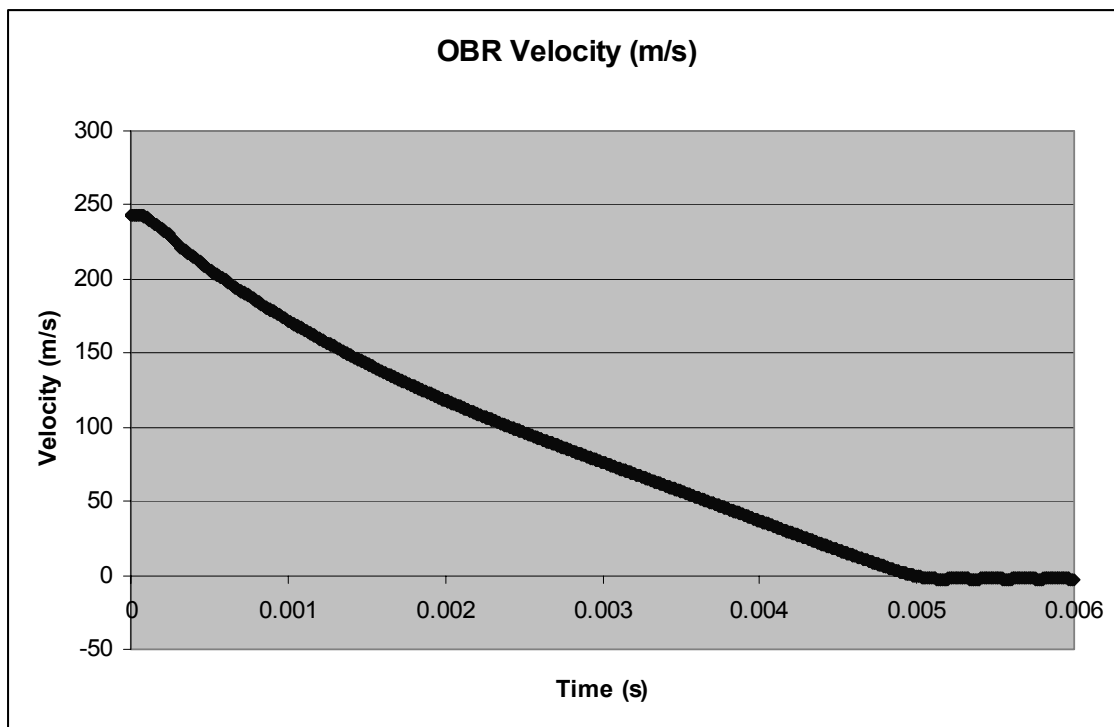
Figure 19. Time history of OBR velocity.

The fast Fourier transforms of the predicted and actual acceleration further confirm the accuracy of the frequency modeling of the simulation. The transforms of the predicted and actual accelerations showed significant peaks at approximately 6,000 Hz and shared similar low-frequency content. This peak at 6,000 Hz represents the frequency content of the OBR, thus verifying the accuracy of the geometric derivation of the OBR's stiffness. The only significant discrepancy between their frequency contents appears around the 12,000-Hz range, where the model predicts an amplitude peak that does not exist. This peak represents the frequency content of the test object, which we had approximated by giving it a stiffness twice that of the OBR. Our approximation was clearly off, and the frequency of the test object should have been in a lower frequency range.

After shot A was conducted, the mitigator was recovered and analyzed. As shown in figure 17, the model predicted that the mitigator would deform 50.6 cm to achieve a final length of 39.6 cm. The actual final length of the mitigator was 38.1 cm, as shown in figure 18. This difference represents a less than 4% error in the prediction of the crush length. It is important to note that the actual mitigator deformed at both its front and rear, while the current model only accounts for deformation at the front of the mitigator. Regardless, the net deformation of the mitigator was accurately predicted.

The model clearly demonstrated the dynamic crush force of the mitigator, since the contour of the acceleration pulse of the model closely follows that of the actual test. The amplitude of the high-frequency oscillations of the current model attenuates more quickly than those of the actual high-frequency oscillations, which indicates that the current model was given too much damping. We can easily fix this error by decreasing the value of ζ in the formulation of the damping coefficients. The identical slopes of the decrease of the predicted and actual acceleration pulses verify the accuracy of the elastic unloading of the mitigator after peak deformation.

5. Future Applications

The current model clearly provides an accurate and improved prediction of the acceleration pulses experienced during air gun testing. However, the complexity of the current model could hinder its implementation because of the greater number of measurements (and therefore time) required to implement it. This is particularly true for the formulation of k-values for the OBR/bird; the geometric calculation of these values requires time-consuming geometric measurements which most researchers do not have time to perform. The calculation of these k-values could be simplified if a simple shock test were conducted on the OBR or test object. If we subject the object to a small impact, its resonant frequency could be discovered and its k-value calculated (*1*) by the equation

$$k = \omega^2 * (M_{\text{Object}}) / 4 \qquad\qquad (19)$$

17

in which ω is the angular frequency of the object. K-values could also be calculated if this test were performed with FE simulation in programs such as ABAQUS. The use of such simulations would produce more accurate results than a geometric formulation but would take a greater amount of time and effort. Overall, the formulation of k-values by means of shock testing would greatly reduce the time required to implement the model, allowing researchers to enjoy a more accurate prediction of acceleration pulses without the requirement of too many additional measurements.

---

6. Conclusion

The current model clearly offers an accurate prediction of the acceleration pulse experienced by a test object during an impact. By accounting for the varying stiffness of the bird as well as the dynamic crush force of the mitigator, the model accurately predicts both the pulse shape and peak acceleration of the bird and test object. It accurately accounts for the frequency content of the test as well. This model is a valuable tool for researchers and, coupled with the time-saving methodologies described before, could be implemented in a time-efficient and practical fashion. The enhanced predictions provided by this model greatly extend the air gun development capabilities of ARL.

7. References

1. Tablei, A.; Chowdhury, M. *ARL Air Gun Modeling and Finite Element Simulation*; TCN #03054; December 2003.

2. Pollin, I. *Impact Pulse Shaping*; ARL Report HDL-TR-1710; June 1975.

3. Bitzer, T. Honeycomb Technology: Materials, Design, Manufacturing, Applications, and Testing. Chapman & Hall: London, 2000.

4. Paz, M. *Structural Dynamics: Theory and Computation*. Reinhold: New York, 1991.

INTENTIONALLY LEFT BLANK

Appendix A. Program Source Code

(Programmed in Visual Basic as a Macro to the Excel Chart included below)

```
Sub ArtSim()

  Dim i As Integer

  Dim k1, k2, k3, delta, M1, m31, m32, m33, yn1, y1, y31, y32, y33, springValue,
mitigatordeflection, maxmitdef As Double
  Dim rho, h, r, rcone, hcone, hcylinder, temp, Area, vcone As Double
  Dim E, L, cPlastic, xPlastic, ec, sigmay, Force As Double
  Dim dforce, kforce, yn31, V0, Mmitigator, Vobr, crushFactor  As Double
  Dim forceCounter As Double
  Dim introwcount As Integer
  Dim c2, c3, Zeta, yPrime2, yPrime3, currentTime, delCounter, maxTime As Double


  k2 = Range("B6")
  k3 = Range("C6")
  delta = Range("E2")
  M1 = Range("A2") + Range("E25")
  m31 = Range("B2")
  m32 = Range("C2")
  m33 = Range("D2")
  Mmitigator = Range("E25")
  rho = Range("E10")
  rcone = Range("E13")
  hcone = Range("E16")
  hcylinder = Range("E19")
  vcone = Range("E28")
  E = Range("E31")
  L = hcone + hcylinder
  xPlastic = 0
  cPlastic = 0
  ec = Range("E37")
  sigmay = Range("E40")
  maxmitdef = 0
  introwcount = Range("H1").CurrentRegion.Rows.Count - 1
  V0 = Range("A28")
  k1 = (3.141592653 * rcone * rcone * E) / L
  Zeta = Range("E43")
  c2 = 2 * Zeta * Math.Sqr(-k2 * (m31 + m32))
  c3 = 2 * Zeta * Math.Sqr(-k3 * (m32 + m33))
  maxTime = Range("E6")
```

```
    'Erase Column
ActiveCell.Value = "Time"
ActiveCell.Offset(1, 0).Select

For i = 1 To introwcount
ActiveCell.Delete
ActiveCell.Offset(1, 0).Select
Next i

' Write time values

delCounter = maxTime / delta
ActiveCell.Offset(-i, 0).Select
ActiveCell.Value = "Time"
ActiveCell.Offset(1, 0).Select

i = 0
currentTime = -delta

For i = 1 To delCounter + 2
    ActiveCell.Value = currentTime
    currentTime = currentTime + delta
    ActiveCell.Offset(1, 0).Select
Next i


introwcount = Range("H1").CurrentRegion.Rows.Count - 1

' Initialize starting positions: t=-delta, 0 (etc)

ActiveCell.Offset(-i, 1).Value = "Y1 (MEM)"
ActiveCell.Offset(-i + 1, 1).Value = -delta * Range("A27")
ActiveCell.Offset(-i + 2, 1).Value = 0
ActiveCell.Offset(-i, 2).Value = "Y31 (OBR Front Plate)"
ActiveCell.Offset(-i + 1, 2).Value = -delta * Range("A28")
ActiveCell.Offset(-i + 2, 2).Value = 0
ActiveCell.Offset(-i, 3).Value = "Y32 (OBR Back Plate)"
ActiveCell.Offset(-i + 1, 3).Value = -delta * Range("A29")
ActiveCell.Offset(-i + 2, 3).Value = 0
ActiveCell.Offset(-i, 4).Value = "Y33 (Test Item)"
ActiveCell.Offset(-i + 1, 4).Value = -delta * Range("A30")
ActiveCell.Offset(-i + 2, 4).Value = 0

ActiveCell.Offset(-i, 5).Value = "Crush Factor"
ActiveCell.Offset(-i, 6).Value = "M31"
```

```
ActiveCell.Offset(-i, 7).Value = "Mitigator Deflection"
ActiveCell.Offset(-i, 10).Value = "Time"
ActiveCell.Offset(-i, 11).Value = "Acceleration (m/s^2)"
ActiveCell.Offset(-i, 12).Value = "Velocity (m/s)"
ActiveCell.Offset(-i, 13).Value = "Acceleration (kG's)"
ActiveCell.Offset(-i, 19).Value = "Time"
ActiveCell.Offset(-i, 20).Value = "Filtered Acceleration"

ActiveCell.Offset(-i + 3, 1).Select

i = 3
For i = 3 To introwcount

    L = hcone + hcylinder - mitigatordeflection

    ActiveCell.Offset(-1, 0).Select
    y1 = ActiveCell.Value
    ActiveCell.Offset(-1, 0).Select
    yn1 = ActiveCell.Value
    ActiveCell.Offset(1, 1).Select
    y31 = ActiveCell.Value
    yn31 = ActiveCell.Offset(-1, 0).Value
    ActiveCell.Offset(0, 1).Select
    y32 = ActiveCell.Value
    ActiveCell.Offset(0, 1).Select
    y33 = ActiveCell.Value
    ActiveCell.Offset(1, -3).Select

    yPrime1 = ((y31 - ActiveCell.Offset(-2, 1).Value) - (y1 - ActiveCell.Offset(-2, _
    0).Value)) / delta
    yPrime2 = ((y32 - ActiveCell.Offset(-2, 2).Value) - (y31 - ActiveCell.Offset(-2, _
    1).Value)) / delta
    yPrime3 = ((y33 - ActiveCell.Offset(-2, 3).Value) - (y32 - ActiveCell.Offset(-2, _
    2).Value)) / delta




    'updates plastic wave speed and location
    cPlastic = (ActiveCell.Offset(-1, 1).Value - ActiveCell.Offset(-2, 1).Value - _
    ActiveCell.Offset(-1, 0).Value + ActiveCell.Offset(-2, 0).Value) / (ec * delta)
    If (cPlastic >= 0) Then
            xPlastic = xPlastic + (cPlastic * delta)
    End If


    mitigatordeflection = y31 - y1
```

```
If (mitigatordeflection < maxmitdef) Then 'And mitigatordeflection < L
        ' After max compression

        'mitigatordeflection = maxmitdef - mitigatordeflection



        Area = 3.141592653 * rcone * rcone
        k1 = -((Area * E) / (L))

        If (forceCounter = 0) Then
                Force = -k1 * (mitigatordeflection - hcone)
                dforce = Force - dforce
                forceCounter = fourcecounter + 1
        End If

        Force = -k1 * (mitigatordeflection - hcone) - dforce



Else
        ' Before max compression
        maxmitdef = mitigatordeflection

        If (xPlastic <= hcone) Then
                h = xPlastic
                Area = (3.141592653 * rcone * rcone) * (h / hcone)
                temp = ((rho * Area * h) / 3#)
                vcone = temp
        Else
                r = rcone
                Area = 3.141592653 * r * r
                h = xPlastic - hcone
                temp = vcone + (rho * Area * h)

        End If



        M1 = Range("A2") + Range("E25") - temp
        m31 = Range("B2") + temp
        k1 = -((Area * E) / L)
        Vobr = (((y31 - yn31) - (y1 - yn1)) / delta)



        crushFactor = (2.627437E-13) * (Vobr * Vobr * Vobr * Vobr * Vobr * Vobr) - _
(0.000000000125438) * (Vobr * Vobr * Vobr * Vobr * Vobr) + (0.0000000159241) * (Vobr * _
Vobr * Vobr * Vobr) + (0.0000005551838) * (Vobr * Vobr * Vobr) - (0.0001897436) * (Vobr _
* Vobr) + (0.008340218) * (Vobr) + 1.257647
```

```
        If (crushFactor < 1) Then
                crushFactor = 1
        End If

        Force = sigmay * Area * crushFactor
        dforce = Force

End If

If (Force < 0) Then
        Force = 0
End If



ActiveCell.Offset(0, 5).Select
ActiveCell.Value = m31
ActiveCell.Offset(0, -5).Select

springValue = ((delta * delta) / M1) * (Force)
ActiveCell.Value = 2 * y1 - yn1 + springValue


ActiveCell.Offset(0, 1).Select

'Calculates y31 displacement


ActiveCell.Offset(-2, 0).Select
yn1 = ActiveCell.Value
ActiveCell.Offset(2, 0).Select

springValue = ((delta * delta) / m31) * (-Force + (k2 * (y31 - y32)) + (c2 * yPrime2))
ActiveCell.Value = 2 * y31 - yn1 + springValue

 'Shift to y32 cell
ActiveCell.Offset(0, 1).Select
'Move to Workspace

ActiveCell.Offset(-2, 0).Select
yn1 = ActiveCell.Value
ActiveCell.Offset(2, 0).Select


springValue = ((delta * delta) / m32) * ((-k2 * y31) + (y32 * (k2 + k3)) - (k3 * y33) – _
(c2 * yPrime2) + (c3 * yPrime3))
```

```vba
ActiveCell.Value = 2 * y32 - yn1 + springValue

'Move to y33 Cell
ActiveCell.Offset(0, 1).Select
ActiveCell.Offset(-2, 0).Select
yn1 = ActiveCell.Value
ActiveCell.Offset(2, 0).Select

springValue = ((delta * delta) / m33) * ((k3 * y33) - (k3 * y32) - (c3 * yPrime3))
ActiveCell.Value = 2 * y33 - yn1 + springValue



ActiveCell.Offset(0, 1).Select
ActiveCell.Value = crushFactor
ActiveCell.Offset(0, -1).Select



ActiveCell.Offset(1, -3).Select

    Next i

ActiveCell.Offset(1, 0).Select
ActiveCell.Value = M1
ActiveCell.Offset(1, 0).Select
ActiveCell.Value = m31
ActiveCell.Offset(-2, 0).Select


MsgBox "Done Calculating Position"

ActiveCell.Offset((-i + 2), 10).Select



Dim j As Integer
Dim un, un1, un2 As Double

'Calculates Y33 Acceleration
For j = 3 To introwcount

        ActiveCell.Offset(-1, -7).Select
        un = ActiveCell.Value
        ActiveCell.Offset(1, 0).Select
        un1 = ActiveCell.Value
        ActiveCell.Offset(1, 0).Select
```

```vba
un2 = ActiveCell.Value
ActiveCell.Offset(-1, 7).Select

ActiveCell.Value = (1# / (delta * delta)) * (un2 + un - 2 * un1)

ActiveCell.Offset(0, 1).Select
ActiveCell.Value = (un2 - un) / (2 * delta)
ActiveCell.Offset(0, -1).Select

ActiveCell.Offset(0, 2).Select
ActiveCell.Value = ActiveCell.Offset(0, -2).Value / -9800
ActiveCell.Offset(0, -2).Select


ActiveCell.Offset(1, 0).Select

Next j

ActiveCell.Offset((-j + 2), 9).Select
MsgBox "Acceleration/Velocity calculations complete."


Dim counter, innercounter As Integer
Dim samplerate As Double
Dim sometemp As Double

samplerate = 1 / (Range("E2") * Range("E34"))

'Calculates Filtered Acceleration
For counter = 3 To (introwcount - (2 * samplerate))
        innercounter = innercounter + 1

        If (innercounter > samplerate) Then
                ActiveCell.Offset(0, -16).Select
                un1 = ActiveCell.Value
                ActiveCell.Offset(-samplerate, 0).Select
                un2 = ActiveCell.Value
                ActiveCell.Offset(2 * samplerate, 0).Select
                un = ActiveCell.Value
                ActiveCell.Offset(-samplerate, 0).Select
                ActiveCell.Offset(0, 16).Select
                ActiveCell.Value = (1# / (delta * delta * samplerate * samplerate)) * (un2 + un - 2_
* un1)

                innercounter = 0
        Else
                ActiveCell.Value = ""
        End If
```

```
        ActiveCell.Offset(1, 0).Select

Next counter

ActiveCell.Offset(-counter + 3, -26).Select


End Sub
```

Excel Table

M1	M31	M32	M33
6.80E+02	4.88E+00	5.49E+00	5.51E+00

K1	K2	K3
-2.00E+08	-6.08E+09	-1.21E+10

Mass Matrix

5.60E+02	0	0	0
0	4.01E+00	0	0
0	0	4.52E+00	0
0	0	0	4.53E+00

Stiffness Matrix

0	0	0	0
0	6.08E+09	-6.08E+09	0
0	6.08E+09	1.82E+10	-1.21E+10
0	0	1.21E+10	-1.21E+10

Inverse Mass Matrix

1.79E-03	0	0	0
0	2.49E-01	0	0
0	0	2.21E-01	0
0	0	0	2.21E-01

Initial Velocity Matrix

0
2.44E+02
2.44E+02
2.44E+02

Final Masses (kg):

M31	M1
8.62391544	564.348

Change in Mass (kg)

M31	M1
4.27E+00	-4.27E+00

Property	Value
Timestep	5.00E-06
Max Time	6.00E-03
Density of Honeycomb	3.85E+02
Radius of Mitigator	0.08811
Length of Wedge Part	0.098298
Length of Cylindrical Part	0.803
Volume of Mitigator	2.2739834E-02
Mass of Mitigator	8.754836E+00
Volume of Conical Mitigator	9.94838E-05
Elastic Modulus of Mitigator	4060000000
Filter Frequency	6250
Compacting Strain	0.64
Yield Stress	2.70E+07
Damping Factor (Zeta)	0.05

Time (s)

Time (s)
-0.000005
0
0.000005
0.00001
0.000015
0.00002
0.000025
0.00003
0.000035
0.00004
0.000045
0.00005
0.000055
0.00006
0.000065
0.00007
0.000075
0.00008
0.000085
0.00009
0.000095
0.0001
0.000105
0.00011
0.000115
0.00012
0.000125
0.00013
0.000135
0.00014
0.000145
0.00015
0.000155
0.00016
0.000165
0.00017
0.000175
0.00018
0.000185
0.00019
0.000195
0.0002
0.000205

Y1 (MEM)	Y31 (OBR Front Plate)	Y32 (OBR Back Plate)	Y33 (Test Item)
0.0000000000E+00	-1.217676600E-03	-1.22E-03	-1.22E-03
0.00E+00	0.000000000E+00	0.0000000000E+00	0
1.59E-09	1.2174524339E-03	1.2176766000E-03	1.2176766000E-03
6.34E-09	2.4344663755E-03	2.4353449365E-03	2.4353532000E-03
1.58E-08	3.6508443114E-03	3.6529835023E-03	3.6530292377E-03
3.16E-08	4.8664113633E-03	4.8705542651E-03	4.8707022726E-03
5.53E-08	6.0810196704E-03	6.0880013875E-03	6.0883658411E-03
8.83E-08	7.2945511663E-03	7.3052519871E-03	7.3060065680E-03
1.32E-07	8.5069187184E-03	8.5222187238E-03	8.5236007700E-03
1.88E-07	9.7180657149E-03	9.7388037791E-03	9.7411109117E-03
2.59E-07	1.0927964285E-02	1.0954903647E-02	1.0958482346E-02
3.44E-07	1.2136612406E-02	1.2170414083E-02	1.2175640785E-02
4.46E-07	1.3344030176E-02	1.3385234576E-02	1.3392490913E-02
5.66E-07	1.4550255560E-02	1.4599271819E-02	1.4608916423E-02
7.06E-07	1.5755339858E-02	1.5812441803E-02	1.5824781654E-02
8.66E-07	1.6959343120E-02	1.7024670377E-02	1.7039934801E-02
1.05E-06	1.8162329696E-02	1.8235892342E-02	1.8254212517E-02
1.26E-06	1.9364363998E-02	1.9446049321E-02	1.9467445562E-02
1.49E-06	2.0565506577E-02	2.0655086828E-02	2.0679465048E-02
1.74E-06	2.1765810522E-02	2.1862951045E-02	2.1890108759E-02
2.03E-06	2.2965318209E-02	2.3069585820E-02	2.3099227014E-02
2.34E-06	2.4164058407E-02	2.4274930370E-02	2.4306687594E-02
2.69E-06	2.5362043771E-02	2.5478918046E-02	2.5512379368E-02
3.07E-06	2.6559268772E-02	2.6681476341E-02	2.6716214374E-02
3.47E-06	2.7755708128E-02	2.7882528174E-02	2.7918128282E-02
3.92E-06	2.8951315832E-02	2.9081994258E-02	2.9118079322E-02
4.40E-06	3.0146024875E-02	3.0279796252E-02	3.0316045901E-02
4.91E-06	3.1339747733E-02	3.1475860249E-02	3.1512023235E-02
5.47E-06	3.2532377710E-02	3.2670120140E-02	3.2706019399E-02
6.06E-06	3.3723791125E-02	3.3862520397E-02	3.3898051193E-02
6.70E-06	3.4913850333E-02	3.5053017882E-02	3.5088140199E-02
7.37E-06	3.6102407475E-02	3.6241582455E-02	3.6276309338E-02
8.09E-06	3.7289308795E-02	3.7428196260E-02	3.7462580114E-02
8.85E-06	3.8474399334E-02	3.8612851778E-02	3.8646970638E-02
9.66E-06	3.9657527737E-02	3.9795548866E-02	3.9829494402E-02
1.05E-05	4.0838550920E-02	4.0976291119E-02	4.1010159695E-02
1.14E-05	4.2017338325E-02	4.2155081992E-02	4.2188969460E-02
1.24E-05	4.3193775538E-02	4.3331921099E-02	4.3365921394E-02
1.34E-05	4.4367767066E-02	4.4506801115E-02	4.4541008069E-02
1.44E-05	4.5539238150E-02	4.5679705587E-02	4.5714216916E-02
1.55E-05	4.6708135545E-02	4.6850607857E-02	4.6885529956E-02
1.66E-05	4.7874427274E-02	4.8019471159E-02	4.8054923266E-02
1.78E-05	4.9038101442E-02	4.9186249800E-02	4.9222366214E-02

Mitigator Deflection	Xplastic
0.000000000000000E+00	1.902619688E-03
1.217450847728170E-03	3.804886637E-03
2.434460034481620E-03	5.706463491E-03
3.650828472775780E-03	7.607039176E-03
4.866379723447670E-03	9.506338005E-03
6.080964381152150E-03	1.140412653E-02
7.294462854224420E-03	1.330021790E-02
8.506786505370720E-03	1.519447360E-02
9.717877239642630E-03	1.708680287E-02
1.092770572413550E-02	1.897715988E-02
1.213626849203940E-02	2.086553921E-02
1.334358421868090E-02	2.275197003E-02
1.454968946007170E-02	2.463650947E-02
1.575463412013520E-02	2.651923550E-02
1.695847686896500E-02	2.840023980E-02
1.816128068044730E-02	3.027962075E-02
1.936310860277420E-02	3.215747688E-02
2.056401982800250E-02	3.403390067E-02
2.176406609290260E-02	3.590897296E-02
2.296328842598600E-02	3.778275785E-02
2.416171425479380E-02	3.965529821E-02
2.535935490032040E-02	4.152661172E-02
2.655620350662050E-02	4.339668767E-02
2.775223347659680E-02	4.526548449E-02
2.894739750284810E-02	4.713292829E-02
3.014162728923090E-02	4.899891233E-02
3.133483405023660E-02	5.086329789E-02
3.252690984964860E-02	5.272591633E-02
3.371772979822480E-02	5.458657250E-02
3.490715507600810E-02	5.644504949E-02
3.609503668407680E-02	5.830111451E-02
3.728121977018300E-02	6.015452558E-02
3.846554832015130E-02	6.200503894E-02
3.964786996871900E-02	6.385241651E-02
4.082804066464910E-02	6.569643323E-02
4.200592892809390E-02	6.753688364E-02
4.318141946339460E-02	6.937358760E-02
4.435441593534850E-02	7.120639459E-02
4.552484277687380E-02	7.303518653E-02
4.669264596492660E-02	7.485987901E-02
4.785779277268460E-02	7.668042089E-02

Time	Acceleration (m/s^2)	Velocity (m/s)	Acceleration (kG's)
-0.000005			
0	0.00E+00	243.53532	0
0.000005	0.00E+00	2.4353532000E+02	0
0.00001	-2.25E+01	2.4353526377E+02	0.002295121
0.000015	-1.20E+02	2.4353490726E+02	0.012256404
0.00002	-3.79E+02	2.4353366034E+02	0.038638085
0.000025	-9.14E+02	2.4353042954E+02	0.09323137
0.00003	-1.86E+03	2.4352349288E+02	0.189897485
0.000035	-3.36E+03	2.4351043437E+02	0.343103172
0.00004	-5.55E+03	2.4348815757E+02	0.566153899
0.000045	-8.52E+03	2.4345298737E+02	0.869364307
0.00005	-1.23E+04	2.4340085674E+02	1.258416617
0.000055	-1.70E+04	2.4332756372E+02	1.733135073
0.00006	-2.24E+04	2.4322907405E+02	2.28685163
0.000065	-2.85E+04	2.4310183785E+02	2.906462741
0.00007	-3.50E+04	2.4294308637E+02	3.573189538
0.000075	-4.18E+04	2.4275107606E+02	4.263965697
0.00008	-4.85E+04	2.4252525305E+02	4.95330017
0.000085	-5.50E+04	2.4226631976E+02	5.61540553
0.00009	-6.10E+04	2.4197619666E+02	6.226353513
0.000095	-6.63E+04	2.4165788350E+02	6.766020561
0.0001	-7.08E+04	2.4131523539E+02	7.219616598
0.000105	-7.43E+04	2.4095267797E+02	7.578645286
0.00011	-7.68E+04	2.4057489138E+02	7.841215742
0.000115	-7.85E+04	2.4018649483E+02	8.011704568
0.00012	-7.94E+04	2.3979176192E+02	8.099842855
0.000125	-7.96E+04	2.3939439130E+02	8.119366096
0.00013	-7.92E+04	2.3899734983E+02	8.086408261
0.000135	-7.86E+04	2.3860279574E+02	8.017840044
0.00014	-7.77E+04	2.3821207993E+02	7.929744213
0.000145	-7.68E+04	2.3782581454E+02	7.836190182
0.00015	-7.59E+04	2.3744399157E+02	7.748420557
0.000155	-7.52E+04	2.3706612998E+02	7.674501602
0.00016	-7.47E+04	2.3669142876E+02	7.61942588
0.000165	-7.43E+04	2.3631890569E+02	7.585597102
0.00017	-7.42E+04	2.3594750581E+02	7.573581788
0.000175	-7.43E+04	2.3557616992E+02	7.582985082
0.00018	-7.46E+04	2.3520386090E+02	7.613301618
0.000185	-7.51E+04	2.3482955215E+02	7.664606565
0.00019	-7.58E+04	2.3445218868E+02	7.7379841
0.000195	-7.68E+04	2.3407063500E+02	7.83563526
0.0002	-7.80E+04	2.3368362582E+02	7.960658059
0.000205	-7.95E+04	2.3328973440E+02	8.116542618

	Time	Filtered Acceleration
	-0.000005	
	0	
	0.000005	
Max Accel	0.00001	
11.99257	0.000015	
	0.00002	
	0.000025	
	0.00003	
	0.000035	
	0.00004	
	0.000045	
	0.00005	
	0.000055	
	0.00006	
	0.000065	
	0.00007	
	0.000075	
	0.00008	
	0.000085	
	0.00009	
	0.000095	
	0.0001	
	0.000105	
	0.00011	
	0.000115	
	0.00012	
	0.000125	
	0.00013	
	0.000135	
	0.00014	
	0.000145	
	0.00015	
	0.000155	-7.24E+04
	0.00016	
	0.000165	
	0.00017	
	0.000175	
	0.00018	
	0.000185	
	0.00019	
	0.000195	
	0.0002	
	0.000205	

2   CDR US ARMY ARDEC
     ATTN AMSTA AR CCH C H CHANIN
          S CHICO
     PICATINNY ARSENAL NJ 07806-5000

1   CDR US ARMY ARDEC
     ATTN AMSTA AR CCH P J LUTZ
     PICATINNY ARSENAL NJ 07806-5000

6   CDR US ARMY ARDEC
     ATTN AMSTA AR CCL F PUZYCKI
          R MCHUGH   D CONWAY
          E JAROSZEWSKI   R SCHLENNER
          M CLUNE
     PICATINNY ARSENAL NJ 07806-5000

3   CDR US ARMY ARDEC
     ATTN AMSTA AR FSA A WARNASH
          B MACHAK M CHIEFA
     PICATINNY ARSENAL NJ 07806-5000

1   CDR US ARMY ARDEC
     ATTN AMSTA AR FSE
     PICATINNY ARSENAL NJ 07806-5000

1   CDR US ARMY ARDEC
     ATTN AMSTA AR FSF T C LIVECCHIA
     PICATINNY ARSENAL NJ 07806-5000

2   CDR US ARMY ARDEC
     ATTN AMSTA AR FSP G M SCHIKSNIS
          D CARLUCCI
     PICATINNY ARSENAL NJ 07806-5000

1   CDR US ARMY ARDEC
     ATTN AMSTA AR M D DEMELLA
     PICATINNY ARSENAL NJ 07806-5000

1   CDR US ARMY ARDEC
     ATTN AMSTA AR QAC T D RIGOGLIOSO
     PICATINNY ARSENAL NJ 07806-5000

1   CDR US ARMY ARDEC
     ATTN AMSTA AR QAC T C J PAGE
     PICATINNY ARSENAL NJ 07806-5000

1   CDR US ARMY ARDEC
     ATTN AMSTA AR TD
     PICATINNY ARSENAL NJ 07806-5000

1   CDR US ARMY ARDEC
     ATTN AMSTA AR WEA   J BRESCIA
     PICATINNY ARSENAL NJ 07806-5000

1   CDR US ARMY ARDEC
     ATTN AMSTA AR WEL F M GUERRIERE
     PICATINNY ARSENAL NJ 07806-5000

1   CDR US ARMY ARDEC
     ATTN AMSTA AR WET T SACHAR
     BLDG 172
     PICATINNY ARSENAL NJ 07806-5000

1   CDR US ARMY ARDEC
     ATTN AMSTA ASF
     PICATINNY ARSENAL NJ 07806-5000

1   CDR US ARMY ARDEC
     PRODUCTION BASE MODERN ACTY
     ATTN AMSMC PBM K
     PICATINNY ARSENAL NJ 07806-5000

1   PM ARMS
     ATTN SFAE GCSS ARMS
     BLDG 171
     PICATINNY ARSENAL NJ 07806-5000

1   PM MAS
     ATTN SFAE AMO MAS
     PICATINNY ARSENAL NJ 07806-5000

1   PM MAS
     ATTN SFAE AMO MAS
     CHIEF ENGINEER
     PICATINNY ARSENAL NJ 07806-5000

1   PM MAS
     ATTN SFAE AMO MAS PS
     PICATINNY ARSENAL NJ 07806-5000

1   PM MAS
     ATTN SFAE AMO MAS LC
     PICATINNY ARSENAL NJ 07806-5000

1   PM MAS
     ATTN SFAE AMO MAS MC
     PICATINNY ARSENAL NJ 07806-5000

1   CDR US ARMY TACOM
     PM ABRAMS
     ATTN SFAE ASM AB
     6501 ELEVEN MILE RD
     WARREN MI 48397-5000

1   CDR US ARMY TACOM
     ATTN AMSTA SF
     WARREN MI 48397-5000

1   CDR US ARMY TACOM
PM BFVS
ATTN SFAE GCSS W BV
6501 ELEVEN MILE RD
WARREN MI 48397-5000

1   CDR US ARMY TACOM
PM SURVIVABLE SYSTEMS
ATTN SFAE GCSS W GSI H M RYZYI
6501 ELEVEN MILE RD
WARREN MI 48397-5000

1   CDR US ARMY TACOM
CHIEF ABRAMS TESTING
ATTN SFAE GCSS W AB QT T KRASKIEWICZ
6501 ELEVEN MILE RD
WARREN MI 48397-5000

1   DIR AIR FORCE RSCH LAB
ATTN MLLMD D MIRACLE
2230 TENTH ST
WRIGHT PATTERSON AFB OH 45433-7817

1   OFC OF NAVAL RESEARCH
ATTN J CHRISTODOULOU
ONR CODE 332
800 N QUINCY ST
ARLINGTON VA 22217-5600

1   US ARMY CERL
ATTN R LAMPO
2902 NEWMARK DR
CHAMPAIGN IL 61822

1   CDR WATERVLIET ARSENAL
ATTN SMCWV QAE Q B VANINA
BLDG 44
WATERVLIET NY 12189-4050

1   TNG DOC & CBT DEV
ATTN ATZK TDD IRSA A POMEY
FT KNOX KY 40121

2   HQ IOC TANK
AMMUNITION TEAM
ATTN AMSIO SMT R CRAWFORD
W HARRIS
ROCK ISLAND IL 61299-6000

1   CDR US ARMY AMCOM
AVIATION APPLIED TECH DIR
ATTN J SCHUCK
FT EUSTIS VA 23604-5577

1   DIR US ARMY AMCOM
ATTN SFAE AV RAM TV D CALDWELL
BLDG 5300
REDSTONE ARSENAL AL 35898

1   NAVAL SURFACE WARFARE CTR
ATTN DAHLGREN DIV CODE G06
DAHLGREN VA 22448

4   CDR US ARMY TACOM
ATTN AMSTA TR R R MCCLELLAND
D THOMAS J BENNETT
D HANSEN
WARREN MI 48397-5000

5   CDR US ARMY TACOM
ATTN AMSTA JSK S GOODMAN
J FLORENCE   A SCHUMACHER
D TEMPLETON   K IYER
WARREN MI 48397-5000

3   CDR US ARMY TACOM
ATTN AMSTA TR D D OSTBERG
L HINOJOSA B RAJU
WARREN MI 48397-5000

2   CDR US ARMY TACOM
ATTN AMSTA CS SF H HUTCHINSON
F SCHWARZ
WARREN MI 48397-5000

10   BENET LABORATORIES
ATTN AMSTA AR CCB R FISCELLA
M SOJA E KATHE M SCAVULO
G SPENCER   P WHEELER
S KRUPSKI J VASILAKIS
G FRIAR R HASENBEIN
WATERVLIET NY 12189-4050

4   BENET LABORATORIES
ATTN AMSTA CCB R S SOPOK
E HYLAND   D CRAYON
R DILLON
WATERVLIET NY 12189-4050

2   US ARMY CORPS OF ENGINEERS
ATTN CERD C T LIU
CEW ET T TAN
20 MASSACHUSETTS AVE NW
WASHINGTON DC 20314

1	US ARMY COLD REGIONS RSCH & ENGRNG LAB ATTN P DUTTA 72 LYME RD HANOVER NH 03755
1	USA SBCCOM PM SOLDIER SPT ATTN AMSSB PM RSS A J CONNORS KANSAS ST NATICK MA 01760-5057
2	USA SBCCOM MATERIAL SCIENCE TEAM ATTN AMSSB RSS J HERBERT M SENNETT KANSAS ST NATICK MA 01760-5057
2	OFC OF NAVAL RESEARCH ATTN D SIEGEL CODE 351 J KELLY 800 N QUINCY ST ARLINGTON VA 22217-5660
1	NAVAL SURFACE WARFARE CTR TECH LIBRARY CODE 323 17320 DAHLGREN RD DAHLGREN VA 22448
1	NAVAL SURFACE WARFARE CTR CRANE DIVISION ATTN M JOHNSON CODE 20H4 LOUISVILLE KY 40214-5245
2	NAVAL SURFACE WARFARE CTR ATTN U SORATHIA C WILLIAMS CD 6551 9500 MACARTHUR BLVD WEST BETHESDA MD 20817-5700
2	CDR NAVAL SURFACE WARFARE CTR CARDEROCK DIVISION ATTN R PETERSON CODE 2020 M CRITCHFIELD CODE 1730 BETHESDA MD 20084
1	NAVAL SURFACE WARFARE CTR CARDEROCK DIVISION ATTN R CRANE CODE 6553 9500 MACARTHUR BLVD WEST BETHESDA MD 20817-5700

3	DIR US ARMY NATL GROUND INTEL CTR
	ATTN D LEITER MS 404
	          M HOLTUS MS 301
	          M WOLFE MS 307
	2055 BOULDERS RD
	CHARLOTTESVILLE VA 22911-8318

3	DIR US ARMY NATL GROUND INTEL CTR
	ATTN S MINGLEDORF MS 504
	          J GASTON MS 301
	          R WARNER MS 305
	2055 BOULDERS RD
	CHARLOTTESVILLE VA 22911-8318

3	DIR US ARMY NATL GROUND INTEL CTR ATTN IANG TMT 2055 BOULDERS RD CHARLOTTESVILLE VA 22911-8318
1	NAVAL SEA SYSTEMS CMD ATTN D LIESE 1333 ISAAC HULL AVE SE 1100 WASHINGTON DC 20376-1100
1	EXPEDITIONARY WARFARE DIV N85 ATTN F SHOUP 2000 NAVY PENTAGON WASHINGTON DC 20350-2000
4	US ARMY SBCCOM SOLDIER SYSTEMS CTR BALLISTICS TEAM ATTN J WARD W ZUKAS J SONG P CUNNIFF KANSAS ST NATICK MA 01760-5019
1	US ARMY SBCCOM SOLDIER SYSTEMS CTR MARINE CORPS TEAM ATTN J MACKIEWICZ KANSAS ST NATICK MA 01760-5019
1	US ARMY SBCCOM SOLDIER SYSTEMS CTR BUS AREA ADVOCACY TEAM ATTN W HASKELL KANSAS ST NATICK MA 01760-5019

2   US ARMY SBCCOM
    SOLDIER SYSTEMS CTR
    ATTN AMSSB RCP SS W NYKVIST
            S BEAUDOIN
    KANSAS ST
    NATICK MA 01760-5019

7   US ARMY RSCH OFC
    ATTN A CROWSON H EVERETT
            J PRATER G ANDERSON
            D STEPP   D KISEROW
            J CHANG
    PO BOX 12211
    RSCH TRIANGLE PARK NC 27709-2211

1   AFRL MLBC
    2941 P ST RM 136
    WRIGHT PATTERSON AFB OH 45433-7750

1   AFRL MLSS
    ATTN R THOMSON
    2179 12TH ST RM 122
    WRIGHT PATTERSON AFB OH 45433-7718

2   AFRL
    ATTN F ABRAMS J BROWN
    BLDG 653
    2977 P ST STE 6
    WRIGHT PATTERSON AFB OH 45433-7739

1   AFRL MLS OL
    ATTN L COULTER
    5851 F AVE
    BLDG 849 RM AD1A
    HILL AFB UT 84056-5713

4   NAVAL SURFACE WARFARE CTR
    ATTN J FRANCIS CODE G30
            D WILSON CODE G32
            R D COOPER CODE G32
            J FRAYSSE CODE G33
    DAHLGREN VA 22448

4   NAVAL SURFACE WARFARE CTR
    ATTN E ROWE CODE G33
            T DURAN CODE G33
            L DE SIMONE CODE G33
            R HUBBARD CODE G33
    DAHLGREN VA 22448

1   DIR LOS ALAMOS NATIONAL LAB
    F L ADDESSIO T 3 MS 5000
    PO BOX 1633
    LOS ALAMOS NM 87545

1   OSD JOINT CCD TEST FORCE
    OSD JCCD
    ATTN R WILLIAMS
    3909 HALLS FERRY RD
    VICKSBURG MS 29180-6199

3   DARPA
    ATTN M VANFOSSEN S WAX
            L CHRISTODOULOU
    3701 N FAIRFAX DR
    ARLINGTON VA 22203-1714

2   SERDP PROGRAM OFC
    PM P2
    ATTN C PELLERIN B SMITH
    901 N STUART ST STE 303
    ARLINGTON VA 22203

3   OAK RIDGE NATL LABORATORY
    ATTN R M DAVIS
            C EBERLE MS 8048
            C D WARREN MS 8039
    PO BOX 2008
    OAK RIDGE TN 37831-6195

4   NIST
    ATTN M VANLANDINGHAM MS 8621
            J CHIN MS 8621
            J MARTIN MS 8621
            D DUTHINH MS 8611
    100 BUREAU DR
    GAITHERSBURG MD 20899

1   HYDROGEOLOGIC INC
    SERDP ESTCP SPT OFC
    ATTN S WALSH
    1155 HERNDON PKWY STE 900
    HERNDON VA 20170

2   NASA LANGLEY RSCH CTR
    ATTN AMSRL VS W ELBER MS 266
            F BARTLETT JR MS 266
    HAMPTON VA 23681-0001

2   NASA LANGLEY RSCH CTR
    ATTN G FARLEY MS 266
            T GATES MS 188E
    HAMPTON VA 23661-3400

1   FHWA
    ATTN E MUNLEY
    6300 GEORGETOWN PIKE
    MCLEAN VA 22101

NO. OF COPIES	ORGANIZATION

1   NATL COMPOSITE CTR
ATTN T CORDELL
2000 COMPOSITE DR
KETTERING OH 45420

3   PACIFIC NORTHWEST LAB
ATTN M SMITH G VAN ARSDALE
         R SHIPPELL
PO BOX 999
RICHLAND WA 99352

4   ALLIANT TECHSYSTEMS INC
ATTN C CANDLAND MN11 2830
        C AAKHUS MN11 2830
        B SEE MN11 2439
        N VLAHAKUS MN11 2145
5050 LINCOLN DR
MINNEAPOLIS MN 55436-1097

4   ALLIANT TECHSYSTEMS INC
ATTN R DOHRN MN11 2830
        S HAGLUND MN11 2439
        M HISSONG MN11 2830
        D KAMDAR MN11 2830
5050 LINCOLN DR
MINNEAPOLIS MN 55436-1097

1   SAIC
ATTN M PALMER
1410 SPRING HILL RD STE 400
MS SH4 5
MCLEAN VA 22102

1   R FIELDS
4680 OAKCREEK ST
APT 206
ORLANDO FL 32835

1   APPLIED COMPOSITES
ATTN W GRISCH
333 NORTH SIXTH ST
ST CHARLES IL 60174

1   CUSTOM ANALYTICAL ENG SYS INC
ATTN A ALEXANDER
13000 TENSOR LANE NE
FLINTSTONE MD 21530

1   AAI CORPORATION
ATTN DR N B MCNELLIS
PO BOX 126
HUNT VALLEY MD 21030-0126

1   OFC DEPUTY UNDER SEC DEFNS
ATTN J THOMPSON
1745 JEFFERSON DAVIS HWY
CRYSTAL SQ 4 STE 501
ARLINGTON VA 22202

3   ALLIANT TECHSYSTEMS INC
ATTN J CONDON E LYNAM
        J GERHARD
WV01 16 STATE RT 956
PO BOX 210
ROCKET CENTER WV 26726-0210

1   PROJECTILE TECHNOLOGY INC
515 GILES ST
HAVRE DE GRACE MD 21078

1   HEXCEL INC
ATTN R BOE
PO BOX 18748
SALT LAKE CITY UT 84118

5   AEROJET GEN CORP
ATTN D PILLASCH T COULTER
        C FLYNN D RUBAREZUL
        M GREINER
1100 WEST HOLLYVALE ST
AZUSA CA 91702-0296

1   HERCULES INC
HERCULES PLAZA
WILMINGTON DE 19894

1   BRIGS COMPANY
ATTN J BACKOFEN
2668 PETERBOROUGH ST
HERNDON VA 22071-2443

1   ZERNOW TECHNICAL SERVICES
ATTN L ZERNOW
425 W BONITA AVE STE 208
SAN DIMAS CA 91773

1   GENERAL DYNAMICS OTS
ATTN L WHITMORE
10101 NINTH ST NORTH
ST PETERSBURG FL 33702

2   GENERAL DYNAMICS OTS
FLINCHBAUGH DIV
ATTN K LINDE T LYNCH
PO BOX 127
RED LION PA 17356

1   GKN WESTLAND AEROSPACE
ATTN D OLDS
450 MURDOCK AVE
MERIDEN CT 06450-8324

5   SIKORSKY AIRCRAFT
ATTN G JACARUSO B KAY
       T CARSTENSAN
       S GARBO MS S330A
       J ADELMANN
6900 MAIN ST
PO BOX 9729
STRATFORD CT 06497-9729

1   PRATT & WHITNEY
ATTN C WATSON
400 MAIN ST MS 114 37
EAST HARTFORD CT 06108

1   AEROSPACE CORP
ATTN G HAWKINS M4 945
2350 E EL SEGUNDO BLVD
EL SEGUNDO CA 90245

2   CYTEC FIBERITE
ATTN M LIN W WEB
1440 N KRAEMER BLVD
ANAHEIM CA 92806

2   UDLP
ATTN G THOMAS M MACLEAN
PO BOX 58123
SANTA CLARA CA 95052

1   UDLP WARREN OFC
ATTN A LEE
31201 CHICAGO RD SOUTH
SUITE B102
WARREN MI 48093

2   UDLP
ATTN R BRYNSVOLD
       P JANKE MS 170
4800 EAST RIVER RD
MINNEAPOLIS MN 55421-1498

2   BOEING ROTORCRAFT
ATTN P MINGURT P HANDEL
800 B PUTNAM BLVD
WALLINGFORD PA 19086

1   LOCKHEED MARTIN
SKUNK WORKS
ATTN D FORTNEY
1011 LOCKHEED WAY
PALMDALE CA 93599-2502

1   LOCKHEED MARTIN
ATTN R FIELDS
5537 PGA BLVD SUITE 4516
ORLANDO FL 32839

1   NORTHRUP GRUMMAN CORP
ELECTRONIC SENSORS & SYSTEMS DIV
ATTN E SCHOCH MS V 16
1745A W NURSERY RD
LINTHICUM MD 21090

1   GDLS DIVISION
ATTN D BARTLE
PO BOX 1901
WARREN MI 48090

2   GDLS
ATTN D REES M PASIK
PO BOX 2074
WARREN MI 48090-2074

1   GDLS
MUSKEGON OPERATIONS
ATTN M SOIMAR
76 GETTY ST
MUSKEGON MI 49442

1   GENERAL DYNAMICS
AMPHIBIOUS SYS
SURVIVABILITY LEAD
ATTN G WALKER
991 ANNAPOLIS WAY
WOODBRIDGE VA 22191

5   INST FOR ADVANCED TECH
ATTN H FAIR I MCNAB
       P SULLIVAN S BLESS
       W REINECKE   C PERSAD
4030-2 W BRAKER LN
AUSTIN TX 78759-5329

1   ARROW TECH ASSO
1233 SHELBURNE RD STE D8
SOUTH BURLINGTON VT 05403-7700

1   R EICHELBERGER
CONSULTANT
409 W CATHERINE ST
BEL AIR MD 21014-3613

1	DREXEL UNIV ATTN A S D WANG 32ND & CHESTNUT ST PHILADELPHIA PA 19104
3	UNIV OF TEXAS AT AUSTIN CTR FOR ELECTROMECHANICS ATTN J PRICE A WALLS J KITZMILLER 10100 BURNET RD AUSTIN TX 78758-4497
1	VA POLYTECHNICAL INST & STATE UNIV DEPT OF ESM ATTN M W HYER K REIFSNIDER R JONES BLACKSBURG VA 24061-0219
1	SOUTHWEST RSCH INST ENGR & MATL SCIENCES DIV ATTN J RIEGEL 6220 CULEBRA RD PO DRAWER 28510 SAN ANTONIO TX 78228-0510
1	BATELLE NATICK OPERATIONS ATTN B HALPIN 313 SPEEN ST NATICK MA 01760

ABERDEEN PROVING GROUND

1	DIRECTOR US ARMY RSCH LABORATORY ATTN AMSRD ARL CI OK (TECH LIB) BLDG 4600
1	US AMSAA ATTN AMXSY TD P DIETZ BLDG 392
1	US ARMY ATC ATTN CSTE DTC AT AC I W C FRAZER BLDG 400
1	DIRECTOR US ARMY RSCH LABORATORY ATTN AMSRD ARL O AP EG M ADAMSON BLDG 245

1	DIRECTOR US ARMY RSCH LABORATORY ATTN AMSRD ARL SL BB D BELY BLDG 328
1	DIRECTOR US ARMY RSCH LABORATORY ATTN AMSRD ARL SL BE W BRUCHEY BLDG 328
3	DIRECTOR US ARMY RSCH LABORATORY ATTN AMSRD ARL WM J SMITH J MCCAULEY M ZOLTOSKI BLDG 4600
1	DIRECTOR US ARMY RSCH LABORATORY ATTN AMSRD ARL WM B (CHIEF) BLDG 4600
1	DIRECTOR US ARMY RSCH LABORATORY ATTN AMSRD ARL WM BA (CHIEF) BLDG 4600
3	DIRECTOR US ARMY RSCH LABORATORY ATTN AMSRD ARL WM BC P PLOSTINS J NEWILL S WILKERSON BLDG 390

7	DIRECTOR
	US ARMY RSCH LABORATORY
	ATTN AMSRD ARL WM BD P CONROY
	     B FORCH M LEADORE R LIEB
	     B RICE R PESCE RODRIGUEZ
	     A ZIELINSKI
	BLDG 4600

1	DIRECTOR US ARMY RSCH LABORATORY ATTN AMSRD ARL WM BD C LEVERITT BLDG 390
1	DIRECTOR US ARMY RSCH LABORATORY ATTN AMSRD ARL WM BF S WILKERSON BLDG 390
2	DIRECTOR US ARMY RSCH LABORATORY ATTN AMSRD ARL WM M S MCKNIGHT J MCCAULEY BLDG 4600

3	DIRECTOR US ARMY RSCH LABORATORY ATTN AMSRD ARL WM MA (CHIEF) L GHIORSE E WETZEL BLDG 4600

22	DIRECTOR
	US ARMY RSCH LABORATORY
	ATTN AMSRD ARL WM MB J BENDER
	    T BOGETTI J BROWN L BURTON
	    R CARTER K CHO W DEROSSET
	    G DEWING R DOWDING
	    W DRYSDALE R EMERSON
	    D GRAY D HOPKINS R KASTE
	    L KECSKES M MINNICINO
	    B POWERS D SNOHA J SOUTH
	    M STAKER J SWAB J TZENG
	BLDG 4600

11	DIRECTOR
	US ARMY RSCH LABORATORY
	ATTN AMSRD ARL WM MC (CHIEF)
	    R BOSSOLI E CHIN
	    S CORNELISON D GRANVILLE
	    B HART J LASALVIA
	    J MONTGOMERY F PIERCE
	    E RIGAS W SPURGEON
	BLDG 4600

11	DIRECTOR
	US ARMY RSCH LABORATORY
	ATTN AMSRD ARL WM MD P DEHMER
	    B CHEESEMAN R DOOLEY
	    G GAZONAS S GHIORSE
	    M KLUSEWITZ W ROY J SANDS
	    D SPAGNUOLO S WALSH
	    S WOLF
	BLDG 4600

2	DIRECTOR US ARMY RSCH LABORATORY ATTN AMSRD ARL WM RP C SHOEMAKER J BORNSTEIN BLDG 1121

1	DIRECTOR US ARMY RSCH LABORATORY ATTN AMSRD ARL WM T B BURNS BLDG 4600

5	DIRECTOR
	US ARMY RSCH LABORATORY
	ATTN AMSRD ARL WM TA W BRUCHEY
	    W GILLICH C HOPPEL
	    M NORMANDIA M ZOLTOSKI
	BLDG 4600

5	DIRECTOR
	US ARMY RSCH LABORATORY
	ATTN AMSRD ARL WM TA T HAVEL
	    J RUNYEON M BURKINS
	    E HORWATH B GOOCH
	BLDG 393

1	DIRECTOR US ARMY RSCH LABORATORY ATTN AMSRD ARL WM TB P BAKER BLDG 390

1	DIRECTOR US ARMY RSCH LABORATORY ATTN AMSRD ARL WM TC R COATES BLDG 309

4	DIRECTOR
	US ARMY RSCH LABORATORY
	ATTN AMSRD ARL WM TD D DANDEKAR
	    M RAFTENBERG S SCHOENFELD
	    T WEERASOORIYA
	BLDG 4600

1	DIRECTOR US ARMY RSCH LABORATORY ATTN AMSRD ARL WM TE (CHIEF) BLDG 1116A

FOREIGN ADDRESSES

1   LTD
R MARTIN
MERL
TAMWORTH RD
HERTFORD SG13 7DG
UK

1   SMC SCOTLAND
P W LAY
DERA ROSYTH
ROSYTH ROYAL DOCKYARD
DUNFERMLINE FIFE KY 11 2XR
UK

1   CIVIL AVIATION
ADMINSTRATION
T GOTTESMAN
PO BOX 8
BEN GURION INTERNL AIRPORT
LOD 70150
ISRAEL

1   AEROSPATIALE
S ANDRE
A BTE CC RTE MD132
316 ROUTE DE BAYONNE
TOULOUSE 31060
FRANCE

1   DRA FORT HALSTEAD
P N JONES
SEVEN OAKS KENT TN 147BP
UK

1   SWISS FEDERAL ARMAMENTS
WKS
W LANZ
ALLMENDSTRASSE 86
3602 THUN
SWITZERLAND

1   DYNAMEC RESEARCH AB
AKE PERSSON
BOX 201
SE 151 23 SODERTALJE
SWEDEN

1   ISRAEL INST OF TECHNOLOGY
S BODNER
FACULTY OF MECHANICAL ENGR
HAIFA 3200
ISRAEL

1   DSTO
WEAPONS SYSTEMS DIVISION
N BURMAN RLLWS
SALISBURY
SOUTH AUSTRALIA 5108
AUSTRALIA

1   DEF RES ESTABLISHMENT
VALCARTIER
A DUPUIS
2459 BOULEVARD PIE XI NORTH
VALCARTIER QUEBEC
CANADA
PO BOX 8800 COURCELETTE
GOA IRO QUEBEC
CANADA

1   INSTITUT FRANCO ALLEMAND
DE RECHERCHES DE SAINT LOUIS
DE M GIRAUD
RUE DU GENERAL
CASSAGNOU
BOITE POSTALE 34
F 68301 SAINT LOUIS CEDEX
FRANCE

1   ECOLE POLYTECH
J MANSON
DMX LTC
CH 1015 LAUSANNE
SWITZERLAND

1   TNO DEFENSE RESEARCH
R IJSSELSTEIN
ACCOUNT DIRECTOR
R&D ARMEE
PO BOX 6006
2600 JA DELFT
THE NETHERLANDS

1   FOA NATL DEFENSE RESEARCH
ESTAB
DIR DEPT OF WEAPONS &
PROTECTION
B JANZON
R HOLMLIN
S 172 90 STOCKHOLM
SWEDEN

1   DEFENSE TECH & PROC AGENCY
GROUND
I CREWTHER
GENERAL HERZOG HAUS
3602 THUN
SWITZERLAND

1   MINISTRY OF DEFENCE
     RAFAEL
     ARMAMENT DEVELOPMENT
     AUTH
     M MAYSELESS
     PO BOX 2250
     HAIFA 31021
     ISRAEL

1   TNO DEFENSE RESEARCH
     I H PASMAN
     POSTBUS 6006
     2600 JA DELFT
     THE NETHERLANDS
     B HIRSCH
     TACHKEMONY ST 6
     NETAMUA 42611
     ISRAEL

1   DEUTSCHE AEROSPACE AG
     DYNAMICS SYSTEMS
     M HELD
     PO BOX 1340
     D 86523 SCHROBENHAUSEN
     GERMANY